

Slow-Speed Supernovae from the Palomar Transient Factory: Two Channels

Christopher J. White,¹ Mansi M. Kasliwal,² Peter E. Nugent,^{3,4} Avishay Gal-Yam,⁵
D. Andrew Howell,^{6,7} Mark Sullivan,⁸ Ariel Goobar,⁹ Anthony L. Piro,¹⁰ Joshua S. Bloom,⁴
Shrinivas R. Kulkarni,¹¹ Russ R. Laher,¹² Frank Masci,¹² Eran O. Ofek,⁵ Jason Surace,¹²
Sagi Ben-Ami,⁵ Yi Cao,¹¹ S. Bradley Cenko,^{13,14} Isobel M. Hook,^{15,16} Jakob Jönsson,¹⁷
Thomas Matheson,¹⁸ Assaf Sternberg,^{19,20} Robert M. Quimby,²¹ Ofer Yaron⁵

ABSTRACT

Since the discovery of the unusual prototype SN 2002cx, the eponymous class of low-velocity, hydrogen-poor supernovae has grown to include at most another two dozen members identified from several heterogeneous surveys, in some cases ambiguously. Here we present the results of a systematic study of 1077 hydrogen-poor supernovae discovered by the Palomar Transient Factory, leading to nine new members of this peculiar class. Moreover we find there are two distinct subclasses based on their spectroscopic, photometric, and host galaxy properties: The “SN 2002cx-like” supernovae tend to be in later-type or more irregular hosts, have more varied and generally dimmer luminosities, have longer rise times, and lack a Ti II trough when compared to the “SN 2002es-like” supernovae. None of our objects show helium, and we counter a previous claim of two such events. We also find that these transients comprise $5.6^{+17}_{-3.7}\%$ (90% confidence) of all SNe Ia, lower compared to earlier estimates. Combining our objects with the literature sample, we propose that these subclasses have two distinct physical origins.

Subject headings: supernovae: general — supernovae: individual (iPTF 13an, PTF 09ego, PTF 09eiy, PTF 09eoi, PTF 10xk, PTF 10bvr, PTF 10ujn, PTF 10acd, PTF 11hyh, SN 2002cx, SN 2002es) — surveys — techniques: spectroscopic

¹Department of Astrophysical Sciences, Princeton University, 4 Ivy Lane, Princeton, NJ 08544, USA

²The Observatories, Carnegie Institution for Science, 813 Santa Barbara Street, Pasadena, CA 91101, USA

³Computational Cosmology Center, Lawrence Berkeley National Laboratory, 1 Cyclotron Road, Berkeley, CA 94720, USA

⁴Department of Astronomy, University of California, Berkeley, CA 94720-3411, USA

⁵Benoziyo Center for Astrophysics, The Weizmann Institute of Science, Rehovot 76100, Israel

⁶Department of Physics, University of California, Santa Barbara, Broida Hall, Mail Code 9530, Santa Barbara, CA 93106-9530, USA

⁷Las Cumbres Observatory Global Telescope Network, Inc., Santa Barbara, CA 93117, USA

⁸School of Physics and Astronomy, University of Southampton, Southampton, SO17 1BJ, UK

⁹The Oskar Klein Centre, Department of Physics, Al-

baNova, Stockholm University, SE-106 91 Stockholm, Sweden

¹⁰Theoretical Astrophysics, California Institute of Technology, 1200 E California Blvd, M/C 350-17, Pasadena, CA 91125, USA

¹¹Cahill Center for Astrophysics, California Institute of Technology, Pasadena, CA 91125, USA

¹²Spitzer Science Center, California Institute of Technology, M/S 314-6, Pasadena, CA 91125, USA

¹³Astrophysics Science Division, NASA Goddard Space Flight Center, Mail Code 661, Greenbelt, MD 20771, USA

¹⁴Joint Space Science Institute, University of Maryland, College Park, MD 20742, USA

¹⁵Department of Physics (Astrophysics), University of Oxford, Keble Road, Oxford OX1 3RH, UK

¹⁶INAF – Osservatorio Astronomico di Roma, Via Frascati 33, 00040, Monte Porzio Catone (RM), Italy

¹⁷Savantic AB, Rosenlundsgatan 50, 118 63 Stockholm, Sweden

¹⁸National Optical Astronomy Observatory, Tucson, AZ

1. Introduction

Thermonuclear supernovae (SNe Ia) have long served as standardizable candles for precision cosmology (Riess et al. 1998; Schmidt et al. 1998; Perlmutter et al. 1999). With the advent of synoptic imaging, the numbers of rare and peculiar supernovae have grown. In particular, many have been found that do not obey the standardization procedure outlined in Phillips (1993), which relates peak luminosity to light curve shape. Here we focus on a class of hydrogen-poor supernovae having the defining feature of unusually low ejecta velocities. This class is identified by similarities to the prototypical member, SN 2002cx (Li et al. 2003), and hence we refer to these objects as O2cx-like.

Perhaps the best studied among O2cx-likes is SN 2005hk (e.g. Chornock et al. 2006; Phillips et al. 2007; Sahu et al. 2008). Roughly two dozen other candidate members have been announced (e.g. Jha et al. 2006; Foley et al. 2013), though about half of these have sparse photometric and spectroscopic coverage. With increased numbers trends have begun to emerge, especially a preference for late-type host galaxies and lower peak luminosities relative to typical SNe Ia. The lowest peak luminosity and lowest velocity belong to the debated member SN 2008ha (Foley et al. 2009, 2010; Valenti et al. 2009). McClelland et al. (2010) claim that SN 2008ha is indeed an O2cx-like based on their discovery of SN 2007qd, whose properties are intermediate between SNe 2002cx and 2008ha. Furthermore, the distinct forest of Co II lines observed in the near infrared by Stritzinger et al. (2014) reinforces the spectroscopic similarity among SN 2008ha, SN 2010ae, and SN 2005hk.

Recently the low-ejecta velocity (slow-speed) and rapidly fading SN 2002es has been reported (Ganeshalingam et al. 2012). This object has ejecta velocities and a peak luminosity similar to SN 2002cx, and it replicates several of SN 2002cx’s characteristic spectral features. However, it is no-

tably different from SN 2002cx in its light curve shape. Furthermore, SN 2002es clearly shows a titanium trough in its spectra—a feature that is not found in SN 2002cx or other members of the developing class. As we discuss in this paper, SN 2002es can be taken as the prototype for an alternate channel leading to low-velocity, hydrogen-poor supernovae.

Here we present slow-speed supernovae discovered by the Palomar Transient Factory (PTF; Rau et al. 2009; Law et al. 2009). Searching through the database of 1077 hydrogen-poor supernovae, we find six new O2cx-like and three new O2es-like transients with velocities less than about 7000 km s⁻¹. We first detail how our final sample of O2cx- and O2es-like objects was chosen in §2. Section 3 contains the analysis of these objects’ properties, divided into host properties (§3.1), photometry (§3.2), spectroscopy (§3.3), the interplay between photometry and spectroscopy (§3.4), and occurrence rates (§3.5). We follow up with a discussion of the implications of our analysis in §4 and present our conclusions in §5.

2. Sample Selection

2.1. The PTF Sample

In order to identify slow-speed supernovae of interest, we thoroughly re-analyzed the spectra in the PTF database. We selected our sample of O2cx- and O2es-like spectra using template matching, after which we further examined the results using ejecta velocities.

First we selected a set of template spectra. We obtained publicly available spectra from the Weizmann Interactive Supernova Data Repository (WiSeREP, see Yaron & Gal-Yam 2012): thirteen of SN 2002cx (Li et al. 2003; Jha et al. 2006), 37 of SN 2005hk (Chornock et al. 2006; Phillips et al. 2007; Blondin et al. 2012), and three of SN 2008ha (Foley et al. 2009). The latter are used as representatives of the extremely low velocity region of the supernova parameter space. Omitting them would risk missing any other such objects, since very low velocities tend to correspond to more lines being resolved, and such spectra may not match even SN 2002cx very well. Furthermore, we included eleven spectra of SN 2002es (M. Ganeshalingam, priv. comm.). The phases for our templates ranged from -8 days to $+314$ days.

85719-4933, USA

¹⁹Excellence Cluster Universe, Technische Universität München, Boltzmannstr. 2, D-85748, Garching, Germany

²⁰Max Planck Institute for Astrophysics, Karl Schwarzschild St. 1, D-85748 Garching, Germany

²¹Kavli IPMU, The University of Tokyo, Kashiwanoha 5-1-5, Kashiwa 277-8583, Japan

For the PTF objects we considered all 1904 hydrogen-poor spectra of 1077 distinct supernovae observed between March 2009 and May 2012. Using the Superfit package (Howell et al. 2005), the spectra were compared to each of 296 supernova spectra in its standard library without any assumptions on phase. Superfit was allowed to choose the redshift that gave the best match in each comparison within ± 0.02 of the PTF best estimate for the actual redshift, sampling in increments of 0.002. Allowing the redshift to vary avoids the situation wherein two otherwise similar spectra are deemed a poor match solely because of differing ejecta velocities. Superfit was also allowed to vary the assumed extinction $A(V)$ between -3 mag and 3 mag, with $R(V)$ fixed at 3.1. The other Superfit settings employed were a 20 Å rebinning of PTF spectra and five iterations of 3σ clipping on a pixel-by-pixel basis to avoid fitting noise. These parameters were found to result in a low false negative rate when tested with known 02cx-likes.

For each PTF supernova, Superfit’s output is a rank-ordered list of matches to templates, using a figure of merit for goodness of fit. Any PTF supernova with a low-velocity template match among the top fifteen matches was selected for further visual inspection. In performing the visual analysis, four features were considered: the number of peaks between 6000 Å and 8000 Å; a particular peak at a rest wavelength of around 6200 Å; the resolution of the feature near 4700 Å into two peaks; and the presence of a Ti II trough. See Figures 1 and 2 for montages of spectra illustrating these features. A summary of the appearance of these features in the final sample can be found in Table 1.

The reason we employ peak counting is that high velocities will tend to smooth spectra and eliminate features. Thus large numbers of peaks serve as a proxy for identifying low velocities. For this inspection we first pass the spectra through a 20 Å Gaussian smoothing filter. This eliminates the high-frequency noise and allows us to unambiguously count features independent of original resolution or signal-to-noise ratio. The smoothed spectra are shown in Figures 3 (02cx-likes) and 4 (02es-likes).

The nature of the 6200 Å feature is not a settled topic in the literature. It may very well be due to adjacent Fe II absorption, as noted by Li

et al. (2003) and Sahu et al. (2008) and modeled by Branch et al. (2004) and Foley et al. (2009). However, it has also been suggested that [Co III] (Li et al. 2003) or O I (McClelland et al. 2010) could play a role.

As a result of visual inspection, there were several Superfit matches we decided were false positives. The PTF targets 11cfm and 11pzq had spectra initially found to match SN 2002cx by Superfit. However, upon further inspection we concluded their spectra were too noisy to justify any certain placement. Furthermore, PTF 11cfm had an ejecta velocity of around 10,000 km s⁻¹. Another preliminary match included PTF 10vzj, but it was rejected upon closer inspection. The last Superfit match that was rejected upon closer inspection is PTF 10xfh (the Type Ic nature of which is discussed in Cao et al., in prep.).

The names and positions of the final sample are given in Table 2. There are nine matches in all, three of which match SN 2002es while the other six match only SN 2002cx. Overlays of spectra from these objects with matching templates can be found in Appendix C. For completeness, each of the nine rejected objects is also given an overlay, in Appendix D, showing the best match we could achieve to a template.

Lest it be thought that the 02cx-likes and 02es-likes are entirely disparate, we note that all three of the SN 2002es matches found were also found to be reasonably good SN 2002cx matches. Indeed, even SN 2002es itself has spectra generally similar to SN 2002cx, resulting in its classification as 02cx-like by Ganeshalingam et al. (2012). At this stage in our analysis these two classes are distinguished only by the visual presence or absence of the Ti II trough, with verification of the dichotomy left to the techniques discussed in §3.

2.2. The Slow-Speed Sample in Context

We place our spectroscopically selected sample in context by constructing a histogram of velocities for all PTF Type Ia supernovae as follows.

First, cuts are made in phase so as to exclude pre-maximum spectra or spectra more than fourteen days post-maximum, as well as any spectra for which there is no reliable phase information. The remaining 837 spectra are deredshifted using the precise spectroscopic redshift of the host

galaxy where available and the approximate supernova redshift otherwise.

Next, each spectrum is plotted and the Si II $\lambda\lambda$ 6348, 6373 absorption feature visually identified. The feature is immediately recognizable in 395 spectra; the other spectra are not considered further in this analysis. The minimum of the feature is compared to the weighted mean of the two rest wavelengths, 6355 Å, and the velocity calculated from this shift is taken to be the ejecta velocity.

Figure 5 shows the distribution of velocities obtained this way for the PTF objects. The histogram also shades the sample ultimately selected for being 02es-like (red) or 02cx-like but not 02es-like (blue), following the procedure of §2.1. The velocities for these selected objects are obtained in a more precise, robust way, as described in Appendix A, comparing the 02cx-likes to the SN 2002cx +12 spectrum, and the 02es-likes to the SN 2002es +6 spectrum. As can be seen, our sample does indeed lie in the low-velocity part of the distribution. Thus there is agreement between the spectrum-matching selection described in the previous section and a simple analysis based solely on an inferred velocity from a single feature.

There were five PTF objects whose Si II velocities were found to be particularly low, but which were nonetheless excluded from our final sample on the basis of being overall poor matches to the templates (overlays shown in Appendix D). The spectrum of PTF 09aly has flat-bottomed profiles, making the velocity obtained too untrustworthy to include in the distribution. Another two objects with low ejecta velocities are PTF 10pko and PTF 10xfv, though both suffer from large uncertainties in host redshift, meaning they could very well be normal SNe Ia scattered into the low-velocity bins by chance. PTF 10pko, moreover, does not show a very clear phase in the spectrum obtained; Superfit finds reasonable matches to templates spanning two weeks in phase. Both PTF 11sd and 09dav have low Si II velocities, but neither shows any spectral similarities to SN 2002cx and company other than just low velocity. Separately we note that PTF 09dav is the lowest-velocity member of a rare class of calcium-rich gap transients (Sullivan et al. 2011; Kasliwal et al. 2012). We choose not to include them because we have no *a priori* reason to believe

all low-velocity objects, no matter how dissimilar their spectra, should be inseparably grouped together.

A detailed analysis of the Si II, Ca II, and C II features in the SN Ia sample from PTF is presented in Maguire et al., in prep.

2.3. The Literature Sample

Recently, Foley et al. 2013 compiled an exhaustive literature sample of 25 supernovae from the past two decades that could potentially be 02cx-likes. We find that the two helium-rich supernovae in this sample, SNe 2004cs and 2007J, are likely not 02cx-like but rather core-collapse Type IIb. As discussed in Appendix B, SN 2004cs shows H α absorption and emission broader than galaxy lines. Furthermore, the light curve of SN 2004cs is consistent with Type IIb (Arcavi et al. 2012). Similarly, SN 2007J shows H α in absorption and is a good spectral match to the prototypical SN IIb 1993J. For more details, we refer the reader to the appendix. Since the two helium-rich objects are fully consistent with hydrogen-rich core-collapse supernovae, we do not consider them to have implications for the physical origin of the 02cx-likes.

In addition to spectral similarity to SN 2002cx, Foley et al. 2013 required the sample to be photometrically “underluminous,” which may include a selection bias against the more luminous, yet kinematically and spectroscopically similar, members of this class. Hence, we combed through the PTF database with a photometry-agnostic sieve.

Given the publicly available data, we are only able to consider ten of the remaining 23 supernovae in this literature sample for comparisons in this paper: SNe 1991bj, 2002cx, 2003gq, 2004gw, 2005hk, 2006hn, 2007qd, 2008ge, 2008ha, and 2009ku. Not all objects have well-sampled photometry and spectroscopy.

3. Analysis

3.1. Host Galaxies

The environment in which a class of supernovae is found can place strong constraints on theories about their progenitors. We present a collage of host galaxies in Figure 6 and summarize host galaxy properties in Table 3.

Comparing the PTF sample of 02cx-likes

(row 2, Figure 6) to the literature sample of 02cx-likes (row 1, Figure 6), we find that the host galaxies are relatively less luminous and more dwarf-like. At the same time the host galaxies of the 02es-likes (row 3, Figure 6) are relatively more luminous and redder than those of the 02cx-likes.

Quantitatively, the R -band luminosities for 02cx-like hosts in the literature range from -17 mag to -21 mag, while our sample ranges from being fainter than -14 mag up to -21 mag. On the other hand, the hosts of 02es-likes span a range of -19 mag to -22 mag. Moreover, the hosts of 02es-likes are redder than $g-i$ of 1.2 mag, while the 02cx-likes’ hosts are on the blue side of this boundary.

There are possible outliers to these overall trends. iPTF 13an has the reddest host of the 02cx-likes; all others have $g-i$ values blueward of 1.0 mag. We note, however, that there are at least two other galaxies close by and at a similar redshift, and it is possible that this supernova in fact belongs to a slightly bluer galaxy. However, SN 2008ge was also reported in a galaxy without significant star formation (Foley et al. 2013), so it may be that 02cx-likes are not restricted to occur *only* in star-forming regions. The implications of this are discussed in §4.3.

Our data indicates a wide range of galaxy properties associated with 02cx-like supernovae, as well as a connection between 02es-like events and luminous galaxies with old stellar populations. To illustrate this graphically, we present a histogram of host types in Figure 7. Because we only have a small sample to work with, we divide host galaxies into just three categories—ellipticals and S0 galaxies, spirals and irregulars, and indeterminate galaxies. Where we cannot find a classification in the literature (i.e. where there is no entry in the last column of Table 3) we fall back to $g-i$ colors to sort bluer galaxies into the spiral category and redder galaxies into the elliptical category. In cases where no data is available we place the object in the “indeterminate” bin.

For comparison, we include in the histogram a sample of generic Type Ia hosts. The data for this population comes from Gallagher et al. (2005), where a set of 57 SNe Ia is studied. The distribution of hosts for 02cx-likes is heavily biased toward star-forming galaxies, whereas 02es-likes tend to be located in early-type hosts. This is reminis-

cent of the observation that overluminous Type Ia supernovae tend to be preferentially found in late-type hosts (Hamuy et al. 1996) when compared to subluminous SNe Ia preferentially found in early-type galaxies (Howell 2001).

3.2. Light Curves

Apparent brightnesses for the PTF targets were obtained in R -band using the 48-inch Samuel Oschin telescope. Image subtraction using the PTFIDE pipeline (Masci 2013, in review) and reference images (Laher et al. 2014, in review) was used to eliminate host light. PSF photometry was performed, calibrated relative to SDSS data (Ofek et al. 2012). The light curves are presented in Figures 8 (for the 02cx-likes) and 9 (for the 02es-likes). Photometric properties can be found in Table 4.

For hosts without redshift-independent distances, distance moduli were calculated from host redshifts assuming a flat cosmology with parameters $H_0 = 70.4 \text{ km s}^{-1} \text{ Mpc}^{-1}$, $\Omega_m = 0.273$, and $\Omega_\Lambda = 0.728$, as given in Jarosik et al. (2011). Applying these to get absolute luminosities, with no corrections made for extinction, one can immediately see that the 02cx-likes’ luminosities span a wide range, from -13 mag to -19 mag. Furthermore, with the inclusion of PTF 09eoi and PTF 10xk, there is no longer such an extreme gap between SN 2008ha and the rest of this class. On the other hand, the well-determined peak luminosities of the 02es-likes are confined to the small range of -17.9 mag to -18.1 mag, toward the bright end of the 02cx-like range.

Some members of the sample were seen early enough to record the rise in the light curve. For simplicity, we fit the pre-maximum datapoints to a parabola. A visual inspection is used to determine which datapoints to use in the fit, but beyond this there is no prior placed on the location of the peak. Here we define the rise time as the time between maximum brightness and when the fit is at 1.5 mag below maximum, and these are the values given in the fourth column of Table 4.¹ We observe a trend of 02cx-like rise times being longer than those of the 02es-likes.

¹Note that the value of 16 days obtained for 02es agrees with the estimate of 16 ± 3 days obtained in Ganeshalingam et al. (2012) using other means.

For most of our sample we are able to measure decline rates. This is simply taken to be the slope of a linear fit to the post-maximum data, where we exclude observations from very late times where the slope of the curve is likely to have changed. The 02cx-likes are seen to have a spread in decline rates, from 0.2 mag to 1.0 mag over the first fifteen days after maximum. Again the spread in properties for the 02es-likes is smaller, lying between 0.57 mag and 0.70 mag over fifteen days.

With multiple properties measured, we can begin to plot the locations of our sample in various slices of parameter space. One set of parameters of particular interest is that of decline rate Δm_{15} and absolute luminosity M . These are the very parameters employed in the Phillips relation (Phillips 1993) that has proven key to cosmology. This plot is shown in Figure 10. For the 02cx-likes, one can see both the offset from typical SNe Ia and the overall diversity of the class reflected in this diagram. The 02es-like objects are also offset in the same way but do not display as much diversity. There is no simple correlation between these two properties in R -band (cf. McClelland et al. 2010).

For aiding comparison, key members of several other proposed sub-classes of supernovae are also plotted. SNe 1991T and 1991bg are prototypical overluminous and underluminous examples, respectively. The former has approximately the same decline rate as our sample, the latter has a similar luminosity, but neither is a particularly good match in this parameter space. We also include a point for SN 2009dc, a so-called super-Chandrasekar Type Ia whose spectrum at one month past maximum is similar to that of SN 2002cx (Silverman et al. 2011). Its location in Figure 10 suggests that it *could* be at the more luminous, slower-declining end of a loose distribution.

We pause to note that most of PTF’s photometry is done in R -band, while decline rates and peak luminosities for normal SNe Ia are often reported in V - and B -bands. We do not have reliable bolometric corrections for the full sample to work in other bands. We caution that working in R -band may cause well known bright events such as SN 2009dc to appear somewhat less luminous. Given that SN 2005hk, for example, was redder post- B -maximum than representative normal and overluminous SNe Ia (cf. Figure 5 in Sahu et al.

2008), it may be that our sample would appear even less luminous next to other Type Ia events if bolometric luminosities or luminosities in bluer bands were used.

3.3. Spectra

We now consider the spectra for these objects. The log of all PTF spectral observations is given in Table 5.

One spectrum for each object is shown in either Figure 1 (02cx-likes) or Figure 2 (02es-likes). These are arranged in order of increasing absolute magnitude from top to bottom, and the features of interest discussed in §2 are highlighted.

In addition to their lack of hydrogen, none of our sample show any clear signs of helium. This is in agreement with the spectral modeling done in Branch et al. (2004), where no helium was needed to match the important features. It is also in accord with the lack of helium in the entire Type Ia sample in Foley et al. (2013) save for SNe 2004cs and 2007J, which we believe do not belong in the same class (see Appendix B).

The most notable difference between the 02cx-likes and 02es-likes is the appearance of the Ti II trough between about 4100 and 4400 Å only in the latter. This feature is simply not present in any of the 02cx-likes, indicating a difference between the two classes in temperature or possibly composition despite ejecta velocity similarities.

For each PTF spectrum in our sample (as well as some other spectra from the literature), we measure the velocities relative to each of six templates (three SN 2002cx spectra, a SN 2005hk spectrum, a SN 2008ha spectrum, and a SN 2002es spectrum) using the method described in Appendix A. The resulting velocity offsets are compiled in Table 6.

Four of the templates have absolute velocities reported from spectral modeling (Branch et al. 2004; Ganeshalingam et al. 2012), enabling us to convert offsets to absolute velocities in these cases. The absolute velocity so obtained will vary depending on the template used. This reflects the fact that the cross-correlation method employed takes into account the entire spectrum, including more lines than just that of Si II. These variations are self-consistent in the sense that, e.g., the change from the first column of offsets to the sec-

ond is always roughly $+1000 \text{ km s}^{-1}$.

From Table 6 one can see that 02es-likes have a range of ejecta velocities (post-maximum) spanning $4000\text{--}7000 \text{ km s}^{-1}$. As has been the case with other properties, the 02cx-likes have a broader range, running from 3000 km s^{-1} to just under $10,000 \text{ km s}^{-1}$.

The velocities slow down over the several weeks following maximum light as expected, but the amount of deceleration varies considerably amongst the 02cx-likes. Two of our 02cx-like supernovae, PTF 09eiy and PTF 09eoi, had spectra taken at many different phases. Figures 11 and 12 show their spectral evolution. The former shows rather clear signs of decreasing velocities, as might be expected from the drop in velocity from roughly 9600 km s^{-1} at $+14$ days to 3900 km s^{-1} at $+121$ days. The features become narrower and more of them are resolved as time passes. In particular, the characteristic 6200 \AA feature grows more distinctive with time. PTF 09eoi, on the other hand, starts with a low velocity, even by SN 2002cx standards, and shows relatively little velocity evolution over a period of approximately 80 days, going from 5400 km s^{-1} at $+21$ days to 4700 km s^{-1} at $+104$ days.

We can also consider the late-phase spectra in their own right. Figure 13 shows five spectra for phases later than $+100$ days obtained for four of the 02cx-like objects in our sample. As was observed by Jha et al. (2006) for the case of SN 2002cx, these objects have many narrow lines indicative of low expansion velocities.

3.4. Combining Photometry and Spectroscopy

When photometric and spectroscopic data is taken together, Arnett’s Law (Arnett 1982) can be used to estimate the mass of the ejecta. In particular, the analysis given in Pinto & Eastman (2000) shows (via their equations 4, 17, and 43) that a plot of magnitude as a function of time is expected to be a parabola near the peak, with

$$m - m_{\text{peak}} \propto -\frac{v_{\text{ej}}}{M_{\text{ej}}\kappa} t^2,$$

where time is measured from the peak and κ is an effective opacity.

Taking normal SN Ia values to be $M_{\text{ej}} = 1.4 M_{\odot}$, $v_{\text{ej}} = 10^4 \text{ km s}^{-1}$, $\kappa = 0.13 \text{ cm}^2 \text{ g}^{-1}$

(as in Pinto & Eastman 2000), and $t_{\text{rise}} = 18$ days (as in Ganeshalingam et al. 2012, whose alternate definition of rise time agrees with ours in the case of SN 2002cx), we can construct curves of constant mass in the $v_{\text{ej}}\text{--}t_{\text{rise}}$ plane for any assumed opacity, as is done in Figure 14. Also plotted are points for members of our sample for which rise times could be computed. These rise times are defined in §3.2 and reported in Table 4. For the ejecta velocities, we use the earliest post-maximum velocity for the event given in Table 6, where for these purposes we use the comparisons to the SN 2002cx $+12$ spectrum for the 02cx-likes, while we use the comparisons to the SN 2002es $+6$ spectrum for the 02es-likes.

From the figure one can immediately infer that the 02cx-likes and 02es-likes must have different ejecta masses and/or opacities. Moreover, even without calculating absolute masses one can see that the 02cx-likes have a broader range of ejecta masses compared to the 02es-likes. In fact, the three 02es-likes fall extremely close to the same contour of constant ejecta mass for any fixed opacity.

Figure 15 shows the relation between *peak* luminosity² and the time evolution of ejecta velocity. One can see that our sample is slow speed in nature even at early phases. Some of the 02cx-likes, such as SN 2003gq (Foley et al. 2013) and PTF 09eiy, show a dramatic change in velocity over the course of several months. Others such as PTF 09ego and PTF 09eoi slow down little over this timeframe. It should be noted here that in some cases but not all, e.g. 09eoi but not 09eiy, the velocity relative to a fixed template increases slightly in the latest phases (see Table 6). As a result, velocities that are only measured infrequently can mask significant evolution.

The peak luminosities are seen to be as diverse as the ejecta velocities; most but not all of the sample luminosities lie below those of typical SNe Ia. Both the 02cx-likes and 02es-likes follow a loose trend of more luminous events having generally faster ejecta.

²Few supernovae have enough spectra to construct a well-sampled, time-dependent curve in velocity-magnitude space.

3.5. Rates

Our data also lends itself to calculating relative rates of slow-speed supernovae in the Type Ia population. Excluding iPTF 13an, which was detected in a different data-taking period than the rest of the sample, we have eight objects at redshifts $z < 0.12$ (Table 3). The PTF database contains 683 SNe Ia within that redshift limit. As the somewhat underluminous nature of these classes means we may miss a greater fraction of them than we do for typical Type Ia supernovae in a volume-limited survey, the rate should be greater than about $8/683 \approx 1\%$. On the other hand, PTF can reliably detect transients at 20.5 mag relative magnitude, and so we should be complete down to an absolute luminosity of -17 mag (-14 mag) by placing an upper limit to the distance modulus of $\mu = 37.5$ mag ($\mu = 34.5$ mag), corresponding to a redshift of $z = 0.070$ ($z = 0.018$). (Here we are assuming negligible extinction.) We detect six (one) slow-speed supernovae out of 304 (eighteen) Type Ia supernovae at $z < 0.070$ ($z < 0.018$). Thus, we can place an upper limit on the rate for supernovae brighter than -17 mag (-14 mag) of 2% (6%). We therefore estimate the rates of slow-speed events in the Type Ia population to be 2.0% if their luminosities are brighter than -17 mag and 5.6% if their luminosities are brighter than -14 mag.

We can take this analysis a step further and give confidence intervals for the rate. Given a rate r , the probability of finding k objects of interest in a sample of N is given by the binomial distribution

$$P_r(k; N) = \binom{N}{k} r^k (1-r)^{N-k}. \quad (1)$$

Assuming a uniform prior on $[0, 1]$, the probability of the rate being less than some value r_0 given an observed fraction k/N is

$$P_{k;N}(r < r_0) = \frac{\int_0^{r_0} P_r(k; N) dr}{\int_0^1 P_r(k; N) dr}. \quad (2)$$

Consider the dimmer cutoff, in which we have $N = 18$, $k = 1$. As $P_{1;18}(r < 31\%) = 99\%$, our rates are significantly lower than the central value of $31^{+17}_{-13}\%$ reported in Foley et al. (2013). Even using the lower end of their interval, $31\% - 13\% = 18\%$, our data predicts the actual rate to be lower with

$P_{1;18}(r < 18\%) = 88\%$ confidence. Note that Foley et al. obtain their rates using correction factors as large as 2, working under the assumption that 02cx-likes are missed more frequently than normal Type Ia events even after limiting the survey volume. Given the homogeneous nature of our survey and data analysis, we do not need to employ such corrections. As $P_{1;18}(r < 23\%) = 95\%$ and $P_{1;18}(r < 1.9\%) = 5\%$, we report a 90% confidence interval for the rate of $5.6^{+17}_{-3.7}\%$. This is consistent with the volume-limited value of 5% quoted in Li et al. (2011).

4. Discussion

4.1. A Summary of the Slow-Speed Sample

Combining the PTF slow-speed sample with the published literature sample, there is an overall dichotomy of properties, with two distinct channels environmentally, photometrically, and spectroscopically (see Table 7). Both channels are low-ejecta velocity explosions of the Type Ia variety (as determined from the features in their hydrogen-poor spectra) with certain additional spectral similarities not found in all SNe Ia. However, there are remarkable differences. SN 2002cx and its closest relatives span a wider range of peak luminosities; have a broader range of ejecta masses and/or opacities; and often appear in late-type hosts, including dwarfs. On the other hand, SN 2002es and related transients display a narrower range of higher peak luminosities; have very similar ejecta masses and opacities; and exclusively reside in luminous, early-type hosts with minimal star formation. Furthermore, despite the otherwise similar spectra, the presence or absence of the Ti II trough is a clear and simple way to discriminate between these two cases.

The Ti II feature is the same one distinguishing faint SN 1991bg-like from brighter SN 1991T-like Type Ia supernovae. It is also remarkable that both 91bg-likes and 02es-likes have older hosts and faster photometric evolution than their counterparts that do not show the Ti II trough. Furthermore the range in peak luminosities is small for both 91bg-likes and 02es-likes.

Reviewing the evidence, both classes share similarities with canonical Type Ia explosions. Contrary to Foley et al. (2013) we believe SNe 2004cs

and 2007J are not related to either class. The distinguishing feature of both our classes is low ejecta velocity, i.e. low kinetic energy per unit ejecta mass. Arnett’s Law, if physically applicable and barring an extreme difference in effective opacity, indicates that O2es-likes have lower masses (see Figure 14), meaning these objects overall have weaker, less energetic explosions. Both classes have somewhat lower peak luminosities relative to typical SNe Ia, and hence have less radioactive material. They both have a rate that is an order of magnitude lower than Type Ia supernovae. Finally, the older environments of the O2es-likes suggest a longer delay time compared to the O2cx-likes.

4.2. Review of Models for SN 2002cx

With these properties in mind, we proceed to discuss the relevant models that have been proposed. When Li et al. (2003) announced the discovery of SN 2002cx, three models were initially put forth as candidates for explaining this event.

The first idea was a variation on the traditional picture of Type Ia supernovae: A single white dwarf explodes as a deflagration and does not immediately transition to a detonation. These models could explain the underluminous, slow-speed nature of SN 2002cx, but they were not fully accepted due to the chemical compositions they predicted. More recent work by Phillips et al. (2007) and Jordan IV et al. (2012), however, has shown that *pure* deflagrations are better candidates for explaining SN 2002cx, with off-center deflagrations leading to appropriate compositions and kinematics. On the other hand, these models cannot explain large ejecta masses, as they leave behind a bound remnant.

The second idea considered by Li et al. is that of two white dwarfs merging—the double-degenerate scenario. Work done by Nomoto et al. (1995) had indicated that the disruption and subsequent accretion of a carbon-oxygen white dwarf onto an oxygen-neon-magnesium white dwarf could result in an underluminous explosion. Attempts were made to explain the low-luminosity supernova SN 1991bg with these models, but they were at the time dismissed in the context of SN 2002cx due to the high expansion velocities they predicted.

The third type of model discussed in Li et al. is that of a low-mass white dwarf being detonated by the ignition of an outer shell of helium. Helium shell detonation has more recently been considered in connection with so-called .Ia models, as discussed in Bildsten et al. (2007). This explanation has the benefit of producing underluminous, hydrogen-poor explosions. However, .Ia explosions are predicted to have ejecta velocities upward of $10,000 \text{ km s}^{-1}$ (Fink et al. 2007; Shen et al. 2010). Moreover, they evolve more rapidly than our observed supernovae, and in fact their rise times are too fast even for SN 2002es (Ganeshalingam et al. 2012). A variation in which accretion from a nondegenerate helium star triggers a deflagration is advocated by Foley et al. (2013) for explaining O2cx-likes, including two supernovae we do not consider to be a part of this class (see §2.3 and Appendix B). We note again that with these objects (which also showed signs of hydrogen) excluded, there is no helium signature in our sample.

We also mention two models not discussed in the original SN 2002cx paper. One recently proposed idea for SN 2002cx events is that of a white dwarf merging with a neutron star or black hole (Fernández & Metzger 2012). Here the white dwarf is spread into an accretion disc vulnerable to detonation waves propagating through it. Of particular interest is the low expansion velocity predicted by such a model, due to the gravity of the compact accreting object. Furthermore, the amount of ^{56}Ni produced is predicted to be less than for a typical Type Ia, leading to low luminosities. In this preliminary stage, however, the model does not yet make specific spectral predictions, and so we cannot yet determine if the spectral features found in O2cx- and O2es-like objects can be obtained from these.

Finally, the possibility has been raised that SN 2008ha is in fact a core-collapse supernova in disguise (Valenti et al. 2009). They note that the core collapse of a hydrogen-deficient star could reproduce the low-luminosity, low-velocity nature of SN 2008ha. Fryer et al. (2009); Moriya et al. (2010) agree, claiming to have a model wherein a large amount of material falls back onto the remnant. One may be tempted to declare SN 2008ha, whose Type Ia status has the most doubt, to be entirely unrelated to SN 2002cx and the other

members of the family. However, as Figures 8 and 15 show, the gap between SNe 2002cx and 2008ha is partially bridged by three supernovae: PTF 10xk, PTF 09eoi, and SN 2007qd (McClelland et al. 2010).

4.3. Two Channels for Two Subclasses

Despite the kinematic and certain spectroscopic similarities between O2cx-likes and O2es-likes, there are enough distinctions to make finding a single, satisfactory model difficult. Considering the observed dichotomy between the two subclasses, we suggest that one should look for two distinct theoretical explanations in order to best fit the two sets of observations.

White dwarf deflagration models are currently favored in the literature for explaining O2cx-likes. We find that some deflagration models may explain the relatively weaker (subluminous and low-energy) O2es-like explosions better than they explain the O2cx-likes.

Recently, Kromer et al. (2013) undertook 3D deflagration simulations of white dwarfs in an attempt to explain O2cx-likes. They found low-velocity and low-luminosity explosions with a small amount of ^{56}Ni (some of which falls back onto a bound remnant). They predict spectra with weak Si II absorption and prominent iron-group elements at all epochs. All four properties are consistent with both O2cx-likes and O2es-likes. However, they note that their model has difficulty being extended far enough to encompass the extremely low ^{56}Ni levels in SN 2008ha. Their rise times are also much shorter than those observed in O2cx-likes.

These latter two shortcomings for explaining O2cx-likes are in fact advantages when it comes to explaining O2es-likes, which have a narrower range of luminosities and shorter rise times. The archetypal model used in that study, N5def, results in $0.372 M_{\odot}$ of ejecta (cf. Figure 14), $0.158 M_{\odot}$ of which is ^{56}Ni , and a rise time of 11.2 days. Furthermore, while Kromer et al. (2013) do not explicitly report on titanium yields or ejecta temperatures, the synthetic spectrum they calculate for two weeks post-maximum (see their Figure 5) shows signs of the same trough we identify as Ti II in O2es-like objects.

Further modeling will be needed to secure what

is now just speculation based on observations of O2es-likes. One key feature any successful model will have to explain is the low scatter in the photometric properties and the preference for older host galaxies seen in this class.

If both O2es-likes and O2cx-likes are deflagrations, then some parameter, e.g. temperature or host environment, must result in distinguishable explosions. Alternatively, O2cx-likes may come from a different channel.

Here we reconsider the double degenerate models for the O2cx-likes. Pakmor et al. (2010) simulate the merger of equal-mass carbon-oxygen white dwarfs and apply this to SN 1991bg. They find low velocities, large amounts of partially burnt material (up to $1.8 M_{\odot}$), and luminosities between -17 mag and -18 mag in R -band. We note that all three features are consistent with both SN 1991bg and the O2cx-likes.

However, the low decline rates found by Pakmor et al. are more consistent with O2cx-likes than SN 1991bg. It is also easier to explain the observed photometric diversity of O2cx-likes in this model—neither white dwarf need be up against the Chandrasekhar limit at the time of merger, so one would expect to see explosions of a range of white dwarf masses. Note that, subject to opacity considerations, our inferred mass for PTF 09ego (see Figure 14) may require the merger of two relatively massive white dwarfs in this scenario.

As Pakmor et al. point out, unless the initial separation is large and/or there is only one common envelope phase, the merger may happen in a relatively short time, while there is still a high rate of star formation in the galaxy. At the same time, some fraction of the appropriate progenitor binaries may have large enough initial separations that by the time the merger does happen, star formation has turned off in the host.

If however the apparently old environment of SN 2008ge is an exception, then the evidence points to young environments rather than a range. This, combined with the fact that there are known core-collapse events with extremely low ejecta velocities (Appendix B), suggests we cannot rule out core-collapse scenarios for O2cx-likes (e.g. fallback; Moriya et al. 2010). Note that PTF 09ego has a large ejecta mass—about $2 M_{\odot}$ with certain opacity assumptions (see Figure 14)—suggesting the

involvement of either two massive white dwarfs or the core collapse of a massive star.

More modeling with 02cx-likes in mind must be done to vet these possibilities. In particular, any successful model must satisfactorily explain the remarkable diversity of this class’s properties, as well as the observed host galaxy distribution.

5. Conclusion

Using the wealth of data obtained over several years of PTF surveys, we were able to identify nine new low-velocity, hydrogen-poor supernovae. Six of these are spectroscopic matches to the much-discussed SN 2002cx, while the other three bear striking similarity to SN 2002es. Combining our sample with those already reported in the literature (which we number at ten), we see a clear dichotomy of properties emerge: The 02cx-likes come from more varied hosts (that are often star-forming), can be quite underluminous, and have hotter ejecta, while the 02es-likes are found in elliptical hosts, are only slightly underluminous, have cooler ejecta, and also have remarkably fast rise times. It is important to note that our selection and classification is based on generic spectral matching; the persistence of the dichotomy through the photometric and host analyses lends further support to the idea that there are indeed two distinct subclasses. Though constituting only $5.6^{+17}_{-3.7}\%$ of Type I supernovae (given the luminosity cut described in §3.5), we now have enough examples of these slow-speed transients to classify and understand them.

Prior attempts at explaining these low-velocity phenomena have fallen notably short of capturing all members. We posit that modeling can be done in a consistent way, but not if one is trying to describe physically distinct scenarios with the same models. The 02cx-likes and the 02es-likes are dissimilar enough to warrant two different progenitor scenarios, and neither class should be confused with hydrogen- or helium-rich transients. Finding a model for 02cx-likes remains difficult, but we speculate that the merger of two carbon-oxygen white dwarfs should at least be considered further now that we have a more coherent picture of this class. More convincingly, there are white dwarf deflagration models that fit observations of 02es-likes. These two channels lead to explosions

that are similar to but distinguishable from typical Type Ia supernovae.

We thank M. H. van Kerkwijk for valuable discussions that improved this manuscript. We also thank I. Arcavi, C. Badenes, V. Bhalerao, K. Clubb, A. Cucchiara, A. De Cia, O. Fox, A. Horesh, D. Levitan, K. Mooley, D. Perley, S. Tang, S. Tendulkar, P. Vreeswijk, and D. Xu for their contributions to PTF, especially with observations and data reduction.

C. J. W. began this research as part of the summer student exchange program between Princeton and Carnegie. M. M. K. acknowledges generous support from the Hubble Fellowship and Carnegie-Princeton Fellowship. A. L. P. is supported through NSF grants AST-1205732, PHY-1068881, and PHY-1151197, as well as the Sherman Fairchild Foundation. E. O. O. is incumbent on the Arye Dissentshik career development chair and is grateful for support by grants from the Willner Family Leadership Institute, Ilan Gluzman (Secaucus, NJ), the Israeli Ministry of Science, the Israel Science Foundation, Minerva, Weizmann-UK, and the I-CORE Program of the Planning and Budgeting Committee and the Israel Science Foundation.

This research made use of the Sloan Digital Sky Survey (SDSS), the NASA/IPAC Extragalactic Database (NED), and the SIMBAD database. The PTF spectra for the slow-speed sample will be made available on WISEREP.

Facilities: PO:1.2m, PO:1.5m, Keck:I (LRIS), Hale (DBSP), ING:Herschel (ISIS), Keck:II (DEIMOS), Magellan:Baade (IMACS)

REFERENCES

- Arcavi, I., et al. 2011, ApJ, 742, L18
- . 2012, ApJ, 756, L30
- Arnett, W. D. 1982, ApJ, 253, 785
- Barbon, R., Benetti, S., Cappellaro, E., Patat, F., Turatto, M., & Iijima, T. 1995, A&A, 110, 513
- Barnes, D. G., et al. 2001, MNRAS, 322, 486
- Bildsten, L., Shen, K. J., Weinberg, N. N., & Nelemans, G. 2007, ApJ, 662, L95
- Blondin, S., et al. 2012, AJ, 143, 126

- Branch, D., Baron, E., Thomas, R. C., Kasen, D., Li, W., & Filippenko, A. V. 2004, *PASP*, 116, 903
- Cappellari, M., et al. 2011, *MNRAS*, 413, 813
- Catinella, B., Haynes, M. P., & Giovanelli, R. 2005, *AJ*, 130, 1037
- Chornock, R., Filippenko, A. V., Branch, D., Foley, R. J., Jha, S., & Li, W. 2006, *PASP*, 118, 722
- de Vaucouleurs, G., de Vaucouleurs, A., H. G. Corwin, J., Buta, R. J., Paturel, G., & Fouqué, P. 1991, *Third Reference Catalogue of Bright Galaxies* (Springer, New York)
- Falco, E. E., et al. 111, *PASP*, 438
- Fernández, R., & Metzger, B. D. 2012, *ArXiv e-prints*
- Filippenko, A. V., et al. 1992, *AJ*, 104, 1543
- Fink, M., Hillebrandt, W., & Röpke, F. K. 2007, *A&A*, 476, 1133
- Fisher, K. B., Huchra, J. P., Strauss, M. A., Davis, M., Yahil, A., & Schlegel, D. 1995, *ApJS*, 100, 69
- Foley, R. J., Brown, P. J., Rest, A., Challis, P. J., Kirshner, R. P., & Wood-Vasey, W. M. 2010, *ApJ*, 708, L61
- Foley, R. J., et al. 2009, *AJ*, 138, 376
- . 2013, *ApJ*, 767, 57
- Fryer, C. L., et al. 2009, *ApJ*, 707, 193
- Gallagher, J. S., Garnavich, P. M., Berlind, P., Challis, P., Jha, S., & Kirshner, R. P. 2005, *ApJ*, 634, 210
- Ganeshalingam, M., et al. 2012, *ApJ*, 751
- Hamuy, M., Phillips, M. M., Schommer, R. A., & Suntzeff, N. B. 1996, *AJ*, 112, 2391
- Howell, D. A. 2001, *ApJ*, 554, L193
- Howell, D. A., et al. 2005, *ApJ*, 634, 1190
- Jarosik, N., et al. 2011, *ApJS*, 192, 14
- Jha, S., Branch, D., Chornock, R., Foley, R. J., Li, W., Swift, B. J., Casebeer, D., & Filippenko, A. V. 2006, *AJ*, 132, 189
- Jones, D. H., et al. 2009, *MNRAS*, 399, 683
- Jordan IV, G. C., Perets, H. B., Fisher, R. T., & van Rossum, D. R. 2012, *ArXiv e-prints*
- Kasliwal, M. M., et al. 2012, *ApJ*, 755, 161
- Kromer, M., et al. 2013, *MNRAS*, 429, 2287
- Laher, R. R., et al. 2014, in review, *PASP*
- Lauberts, A., & Valentijn, E. A. 1989, *The surface photometry catalogue of the ESO-Uppsala galaxies* (Garching: European Southern Observatory)
- Law, N. M., et al. 2009, *PASP*, 121, 1395
- Li, W., Singer, D., Boles, T., & LOSS/KAIT. 2004, *IAU Circ.*, 8361
- Li, W., et al. 2003, *PASP*, 115, 453
- . 2011, *MNRAS*, 412, 1441
- Lira, P., et al. 1998, *AJ*, 115, 234
- Lu, N. Y., Hoffman, G. L., Groff, T., Roos, T., & Lamphier, C. 1993, *ApJS*, 88, 383
- Masci, F. 2013, in review, *PASP*
- McClelland, C. M., et al. 2010, *ApJ*, 720, 704
- Moriya, T., et al. 2010, *ApJ*, 719, 1445
- Narayan, G., et al. 2011, *ApJ*, 731, L11
- Nomoto, K., Iwamoto, K., Yamaoka, H., & Hashimoto, M. 1995, in *ASP Conference Series*, Vol. 72, *Millisecond Pulsars: A Decade of Surprise*, ed. A. S. Fruchter, M. Tavani, & D. C. Backer, ASP, San Francisco, CA, 164–174
- Ofek, E. O., et al. 2012, *PASP*, 124, 62
- Ogando, R. L. C., Maia, M. A. G., Pellegrini, P. S., & da Costa, L. N. 2008, *AJ*, 135, 2424
- Pakmor, R., Kromer, M., Röpke, F. K., Sim, S. A., Ruiter, A. J., & Hillebrandt, W. 2010, *Nature*, 463, 61
- Pastorello, A., et al. 2008, *MNRAS*, 389, 955

- Paturel, G., Theureau, G., Bottinelli, L., Gouguenheim, L., Coudreau-Durand, N., Hallet, N., & Petit, C. 2003, *A&A*, 412, 57
- Perlmutter, S., et al. 1999, *ApJ*, 517, 565
- Phillips, M. M. 1993, *ApJ*, 413, L105
- Phillips, M. M., et al. 2007, *PASP*, 119, 360
- Pinto, P. A., & Eastman, R. G. 2000, *ApJ*, 530, 744
- Prieto, J. L., Rest, A., & Suntzeff, N. B. 2006, *ApJ*, 647, 501
- Rajala, A. M., et al. 2005, *PASP*, 117, 132
- Rau, A., et al. 2009, *PASP*, 121, 1334
- Riess, A. G., et al. 1998, *AJ*, 116, 1009
- Sahu, D. K., et al. 2008, *ApJ*, 680, 580
- Schmidt, B. P., et al. 1998, *ApJ*, 507, 46
- Shen, K. J., Kasen, D., Weinberg, N. N., Bildsten, L., & Scannapieco, E. 2010, *ApJ*, 715, 767
- Silverman, J. M., Ganeshalingam, M., Li, W., Filippenko, A. V., Miller, A. A., & Poznanski, D. 2011, *MNRAS*, 410, 585
- Strauss, M. A., Huchra, J. P., Davis, M., Yahil, A., Fisher, K. B., & Tonry, J. 1992, *ApJS*, 83, 29
- Stritzinger, M. D., et al. 2014, *A&A*, 561, A146
- Sullivan, M., et al. 2011, *ApJ*, 732, 118
- Tonry, J., & Davis, M. 1979, *AJ*, 84, 1511
- Valenti, S., et al. 2009, *Nature*, 459, 674
- Yaron, O., & Gal-Yam, A. 2012, *PASP*, 124, 668

A. Obtaining Robust Velocities via Cross-Correlation

Here we describe our method for measuring precise relative velocities between an input spectrum and a template. This method is robust against weak Si II lines being difficult to discern amongst many low-velocity features. Each input is compared to the appropriate template using the IRAF routine `fxcor`. The theory behind the routine is given in Tonry & Davis (1979), and we summarize the idea of the procedure and our usage of it here.

First, all spectra are de-redshifted according to their hosts' cataloged redshifts (as listed below in Table 3). They are then rebinned to a rest frame resolution of 1 \AA , which is in all cases finer than the raw data. Spectra are continuum subtracted with a cubic spline averaged over five points, rejecting data points at the 2σ level. Five iterations are performed with a one-pixel grow radius.

Next, the spectra are limited to the wavelength range of $4000\text{--}7000 \text{ \AA}$. This was chosen as the maximal range covered by all object and template data. For both the object and the template, this windowed spectrum is Fourier transformed with periodic boundary conditions, apodizing 20% of the window with a cosine bell on either end to prevent discontinuity artifacts stemming from the enforced periodicity. The spectra are then filtered by multiplying these transforms by a ramp function. The ramp rises from zero to unity between wavenumbers 10 and 15, filtering out very low frequency variations. It descends back to zero over the wavenumber range $1067\text{--}1600$, excluding any signal with a frequency more than about half the highest achievable spatial frequency given the resolution.

As described in Tonry & Davis (1979), one takes the product of the Fourier transforms and fits a symmetric function—in our case a Gaussian—to the largest peak in this correlation function; the center corresponds to the relative velocity. In practice we identify the peak of interest as the largest one with a reasonable shift—i.e., the ejecta velocity must be positive and is almost certainly less than $20,000 \text{ km s}^{-1}$ —and fit this peak to a Gaussian as follows. The peak is defined as the contiguous set of points with values at least half that of the largest value in the peak. Each datapoint, corresponding to a single wavenumber, is weighted by a symmetric triangle function that vanishes at the outermost points and reaches its maximum of unity at the center. A least-squares fit is then performed, with the model being a Gaussian with no offset. The shifts of the peaks directly translate into relative ejecta velocities, and these are tabulated in Table 6. More information could in theory be ascertained from the shape of the peak, but for our purposes here we only use the relative velocity thus obtained.

This method has the advantage of taking all lines into account. Furthermore, the weighting of the lines in contributing to the final velocity scales quadratically in the amplitude of the line. As discussed in Tonry & Davis (1979), this is a desired feature.

B. The Type IIb Nature of SNe 2004cs and 2007J

SN 2004cs was discovered by LOSS (Li et al. 2004) and classified as a Type IIb supernova by Rajala et al. (2005) based on a Keck/LRIS spectrum now available on WISEREP. This spectrum showed strong He I features, as well as the $H\alpha$ line. Recently, Foley et al. (2013) reanalyzed the spectrum, claiming the $H\alpha$ feature consists only of host galaxy emission that is furthermore blueshifted compared to nearby lines. They associate this object with the class of 02cx-likes via comparison with SN 2007J. This association is then used to bolster the claim, originally based only on SN 2007J, that some members of this class show helium signatures and that therefore the class as a whole must come from progenitor systems that contain an abundant source of helium (e.g. accreting binary systems with helium star donors).

Due to the importance of this issue, we reexamine these two objects here. The spectrum of SN 2004cs is shown in Figure 16. In addition to prominent He I absorption lines, the object displays the $H\alpha$ line, both in emission (broader than galaxy lines) and absorption. This line is blueshifted with respect to the host lines and is thus unaffected by possible host galaxy contamination.

In order to clarify line identification, we went through the PTF database and located the two Type IIb

supernovae with the lowest expansion velocities. One of those, PTF 10qrl, has a spectrum similar to that of SN 2004cs, though its expansion velocities are not as low. PTF 10qrl has a very strong and obvious $H\alpha$ line, as well as higher order Balmer lines ($H\beta$ and $H\gamma$) and He I lines, so its Type IIb classification is not in question. This spectrum is also plotted in Figure 16, after being redshifted by 3000 km s^{-1} . As can be seen, the spectra are quite similar, with most features aligning very well. The expansion velocity is indeed somewhat higher for hydrogen than for He I, but this is a known feature of SNe IIb (e.g. Arcavi et al. 2011) reflecting the fact that the thin hydrogen layer lies above the deeper helium-rich layers, and the velocity difference seen in PTF 10qrl is the same as that seen in SN 2004cs.

To further illuminate this issue, we recall the process through which the class of O2cx-likes was associated with SNe Ia: spectral comparison of artificially broadened and blueshifted low-velocity spectra with those of normal events (e.g. in Figure 1 of Foley et al. 2013). We repeat this process for SN 2004cs, convolving the spectrum with a 50 \AA Gaussian filter and blueshifting the result by 3000 km s^{-1} . Figure 16 compares the result with a spectrum of the prototypical Type IIb SN 1993J (Barbon et al. 1995, available on WISEREP), and the similarity is striking throughout the entire visible wavelength range, including the clear alignment of the $H\alpha$ absorption features.

Regarding the light curve of SN 2004cs, Figure 16 of Foley et al. (2013) shows this object being something of an outlier in terms of a width-luminosity relation in V -band that may exist for the O2cx-likes. We therefore investigate whether the photometry for this object can shed light on its nature. Arcavi et al. (2012) show that SNe IIb have a very tight range of decline rates in R -band. In Figure 17 we overlay the light curve of SN 2004cs (Foley et al. 2013, we follow the common practice of assuming unfiltered KAIT datapoints trace R -band luminosity) on the Arcavi et al. (2012) SN IIb template, finding good agreement.

We conclude that SN 2004cs is indeed a Type IIb supernova, as it was originally classified by Rajala et al. (2005). The spectrum provides strong support for this classification, including robust evidence for hydrogen. The photometry provides further support, showing this object to be consistent with SNe IIb rather than O2cx-like SNe Ia.

Motivated by our study of SN 2004cs, we now turn to SN 2007J, the similarity to which led Foley et al. (2013) to classify the former as an O2cx-like. In Figure 18 we compare the spectrum of SN 2007J to the Type IIb SN 1993J. The spectra are indeed quite similar. In particular, an absorption line coincident with $H\alpha$ can be seen in the SN 2007J spectrum. The expansion velocity derived from this feature assuming it is $H\alpha$ is 9000 km s^{-1} , which is greater than the He I velocity (6500 km s^{-1}), as we have already noted is commonly seen in SNe IIb. One may argue that there is no corresponding $H\beta$ feature in the SN 2007J spectrum, but this has also been seen in some SNe IIb (e.g. SN 2008ax, see Pastorello et al. 2008, Figure 5) and probably suggests that the amount of hydrogen is lower in this object than in SN 1993J.

From this analysis we conclude that SN 2007J could also be a Type IIb supernova, rather than an O2cx-like Type Ia. We therefore view the claim of a helium connection to the O2cx-class—a connection based only on SN 2004cs and SN 2007J—as questionable. The helium in these two objects should not be taken as a constraint on the progenitor systems of O2cx-like transients.

C. Individual Spectra

Here we present overlays showing the matches between our PTF spectra and SN 2002cx or SN 2002es, as is appropriate. We show a single phase for each PTF object, and the template against which we choose to match it is chosen based on the phase of our spectrum.

D. Spectra of Objects Determined to Not Match

Here we present overlays for the nine rejected objects discussed in §2.1. The first four objects—PTF 10vzj, 10xfh, 11cfm, and 11pzq—were automatically flagged by Superfit but did not pass further scrutiny. The

other five are examples of slow-speed supernovae that are poor spectral matches to SN 2002cx, SN 2002es, or other related objects. Each overlay shows the best match we could get to an 02cx-like or SN 2002es template of interest.

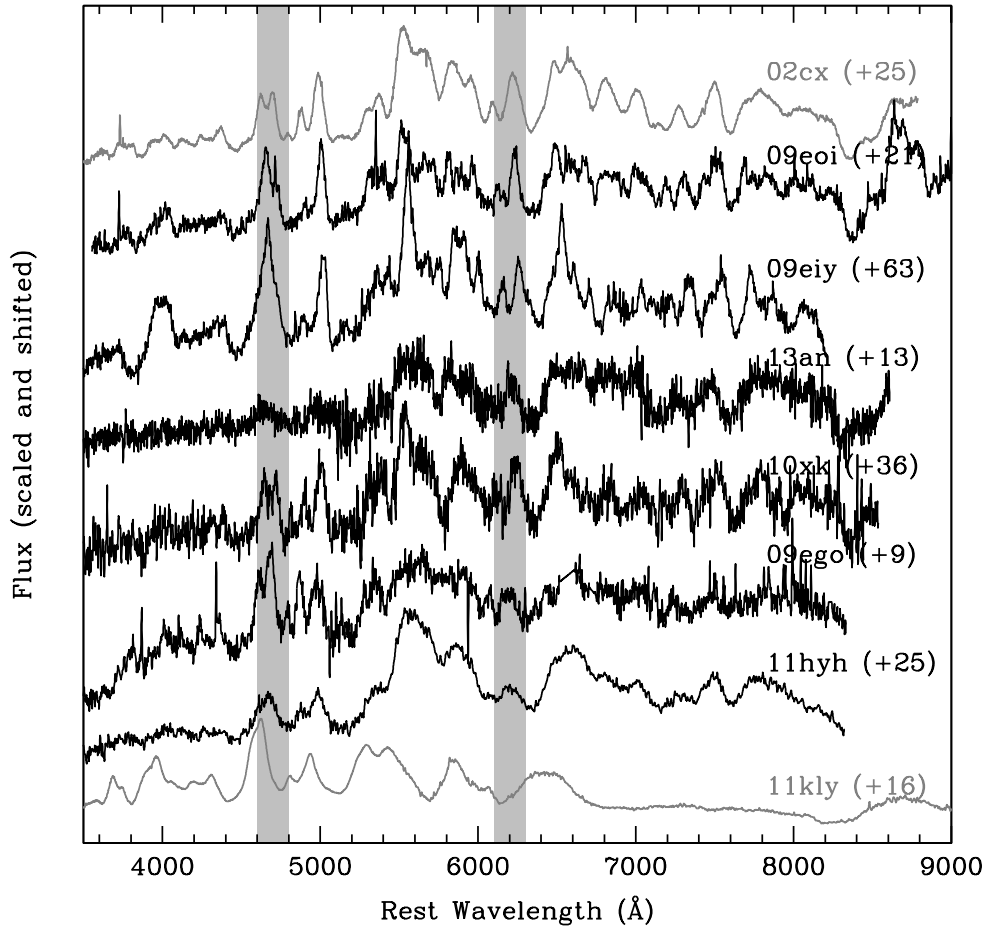


Fig. 1.— Montage of confirmed 02cx-like spectra. SN 2002cx is shown on top, with a typical SN Ia shown at the bottom. The gray bands highlight regions of particular interest. Details of observations can be found in Table 5.

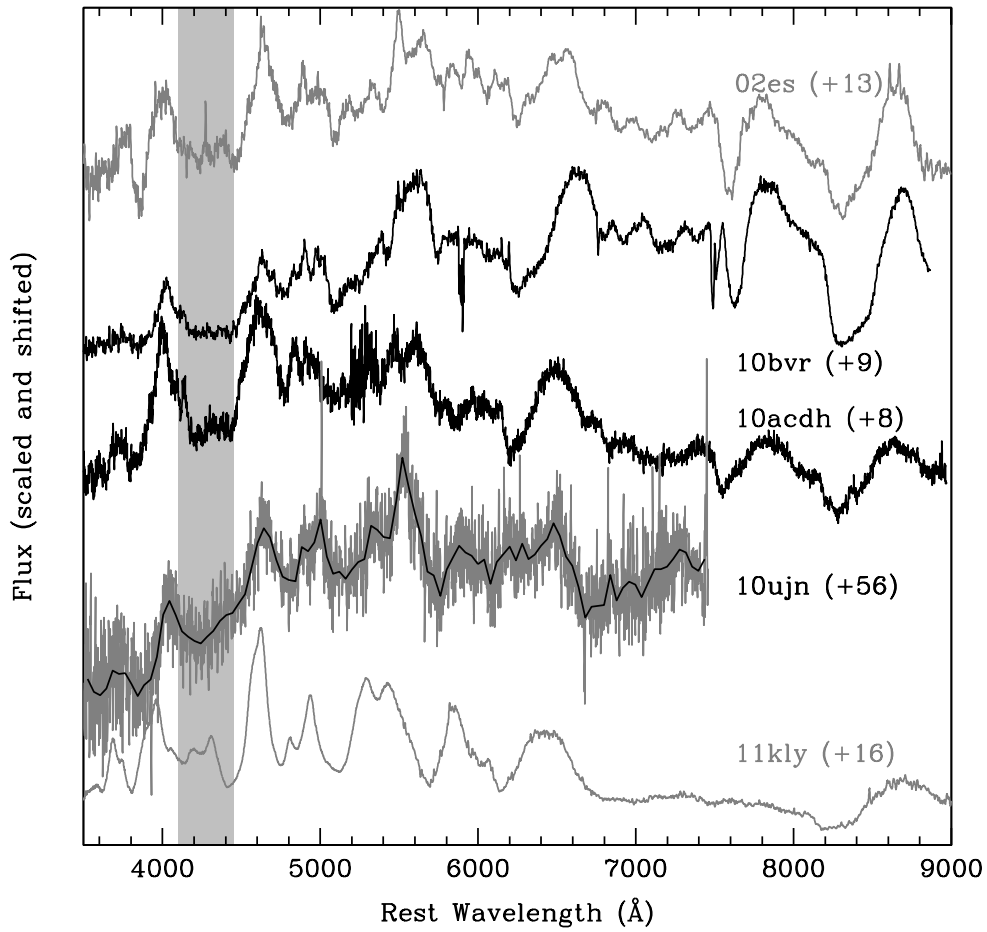


Fig. 2.— Montage of 02es-like spectra. SN 2002es is shown on top, with a typical SN Ia shown at the bottom. The gray band highlights the titanium trough. The PTF 10ujn spectrum has been binned for clarity. Details of observations can be found in Table 5.

TABLE 1
VISUAL VETTING

Name	Phase (days)	# Peaks (6000–8000 Å) ^a	4700 Å Resolved?	6200 Å Feature?	Ti II Trough?
Templates					
SN 2002cx	+25	9	yes	yes	no
SN 2002es	+13	12	no	yes	yes
SN 2011fe	+16	2	no	no	no
02cx matches					
PTF 09ego	+9	6+	yes	yes	no
PTF 09eiy	+55	5+	no	yes	no
PTF 09eoi	+38	12	yes	yes	no
PTF 10xk	+31	12	yes	yes	no
PTF 11hyh	+23	7	no	yes	no
iPTF 13an	+13 ^b	11	yes	yes	no
02es matches					
PTF 10bvr	+9	8	maybe	maybe	yes
PTF 10ujn	+119	9+	no	maybe	maybe
PTF 10acdh	+42	7	no	maybe	yes
False positives					
PTF 09aly	+6	4	no	no	no
PTF 10pko	+8	14	yes	no	no
PTF 10vzj	+51	10	yes	no	no
PTF 10xfh	...	10	maybe	yes	yes
PTF 10xfv	+17	13	maybe	no	no
PTF 11sd	+8	6	no	no	no
PTF 11cfm	+24	8+	maybe	no	no
PTF 11pzq	+18	9	no	no	no

^aA “+” indicates the spectrum does not fill the entire range and so a more complete spectrum would likely have more points. The counting is performed using the spectra as shown in Figures 3 and 4.

^bAssumes first observation corresponds to peak brightness.

TABLE 2
PTF SAMPLE POSITIONS

Name	RA (J2000)	DEC (J2000)
PTF 09ego	17 ^h 26 ^m 25.16 ^s	+62°58′22.1″
PTF 09eiy	01 ^h 54 ^m 16.68 ^s	−15°05′01.6″
PTF 09eoi	23 ^h 24 ^m 12.87 ^s	+12°46′42.6″
PTF 10xk	01 ^h 41 ^m 02.86 ^s	+30°13′38.7″
PTF 10bvr	16 ^h 31 ^m 18.85 ^s	+39°09′20.4″
PTF 10ujn	07 ^h 53 ^m 13.72 ^s	+72°20′13.5″
PTF 10acdh	09 ^h 43 ^m 07.58 ^s	+09°39′31.3″
PTF 11hyh	01 ^h 45 ^m 50.50 ^s	+14°35′00.0″
iPTF 13an	12 ^h 14 ^m 15.35 ^s	+15°32′09.6″

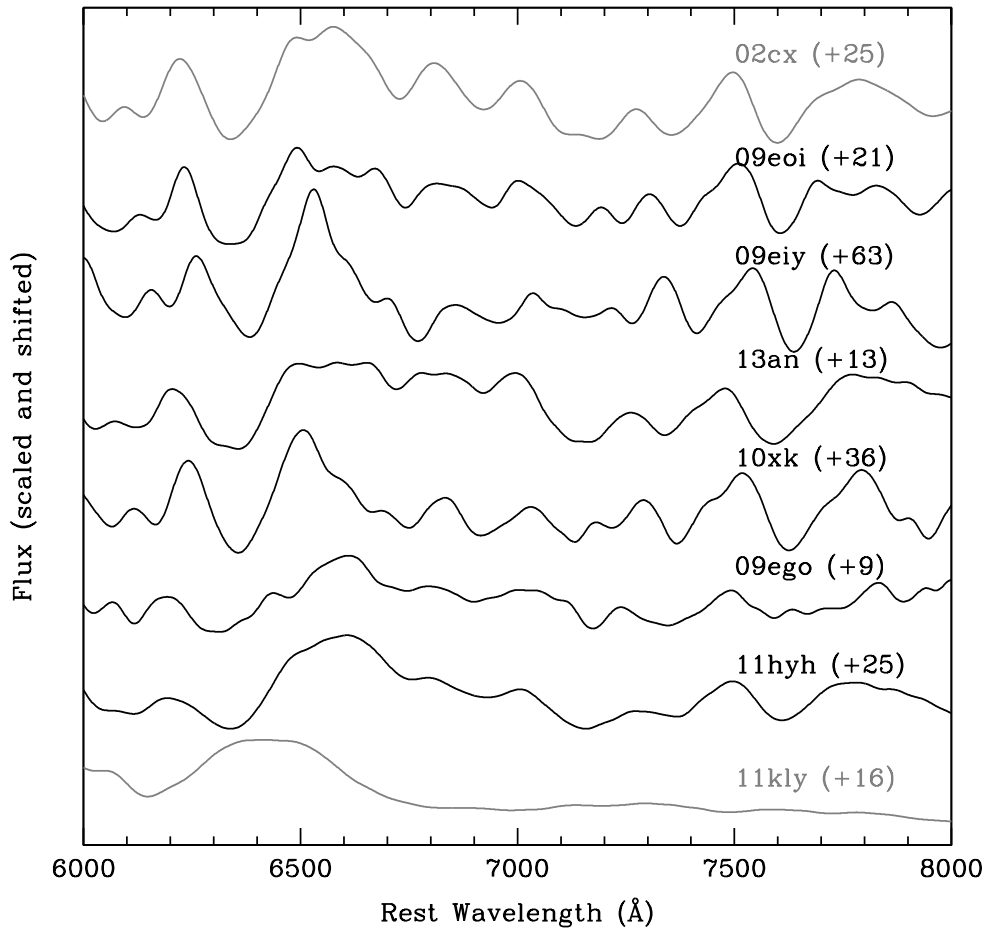


Fig. 3.— Montage of confirmed 02cx-like spectra, focusing on 6000–8000 Å and smoothed with a Gaussian filter of standard deviation 20 Å. SN 2002cx is shown on top, with a typical SN Ia shown at the bottom. Details of observations can be found in Table 5.

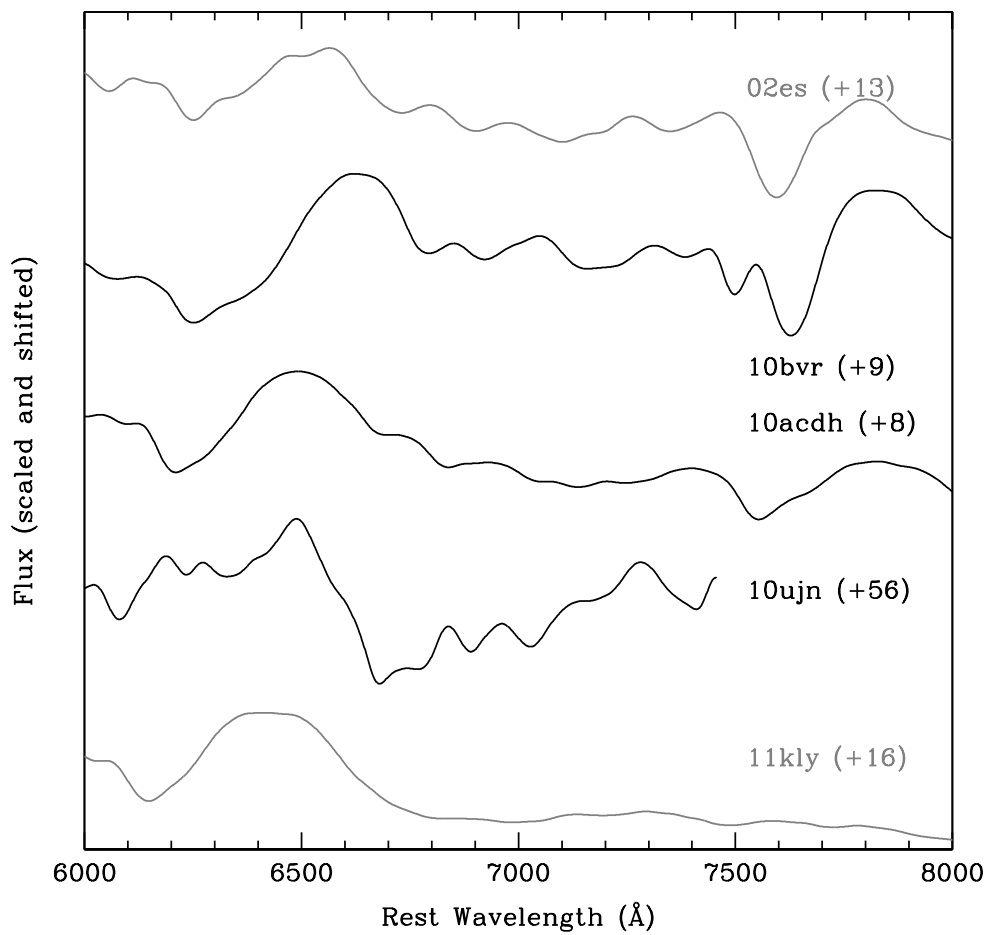


Fig. 4.— Same as Figure 3, but showing the matches to SN 2002es.

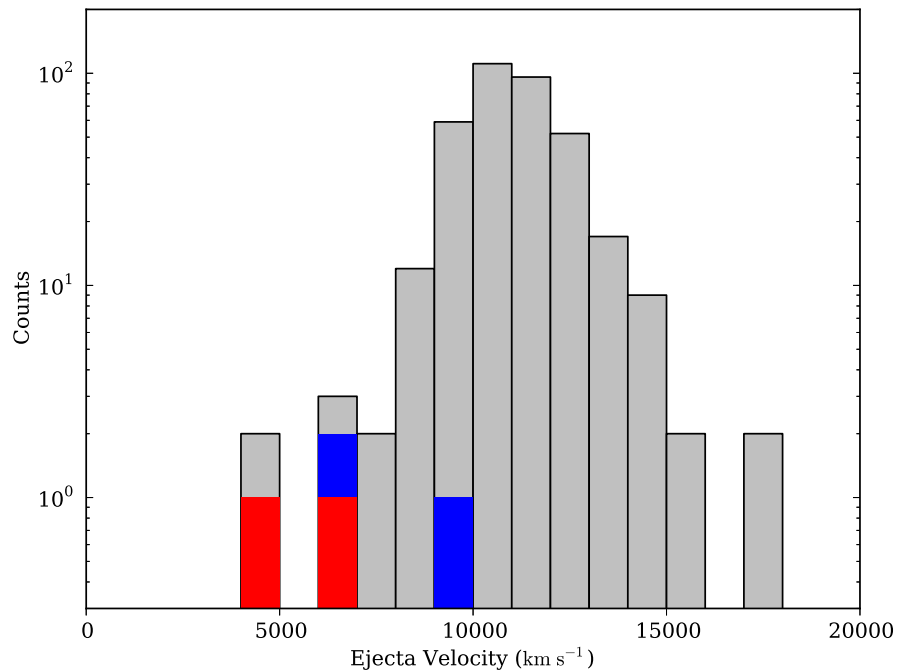


Fig. 5.— Distribution of ejecta velocities in PTF data. Shown are SNe with phases ranging from maximum brightness to +14 days. The blue region denotes the 02cx-like objects, with the red section counting the 02es-likes. Velocities are averaged in the case of multiple spectra for the same object. Note that many of our 02cx-like and 02es-like spectra are excluded here in adherence to our strict phase cut. Some objects, such as PTF 10pko (4100 km s^{-1}) and PTF 11sd (6800 km s^{-1}), have low expansion velocities but are not 02cx-like or 02es-like, as discussed in §2.2.

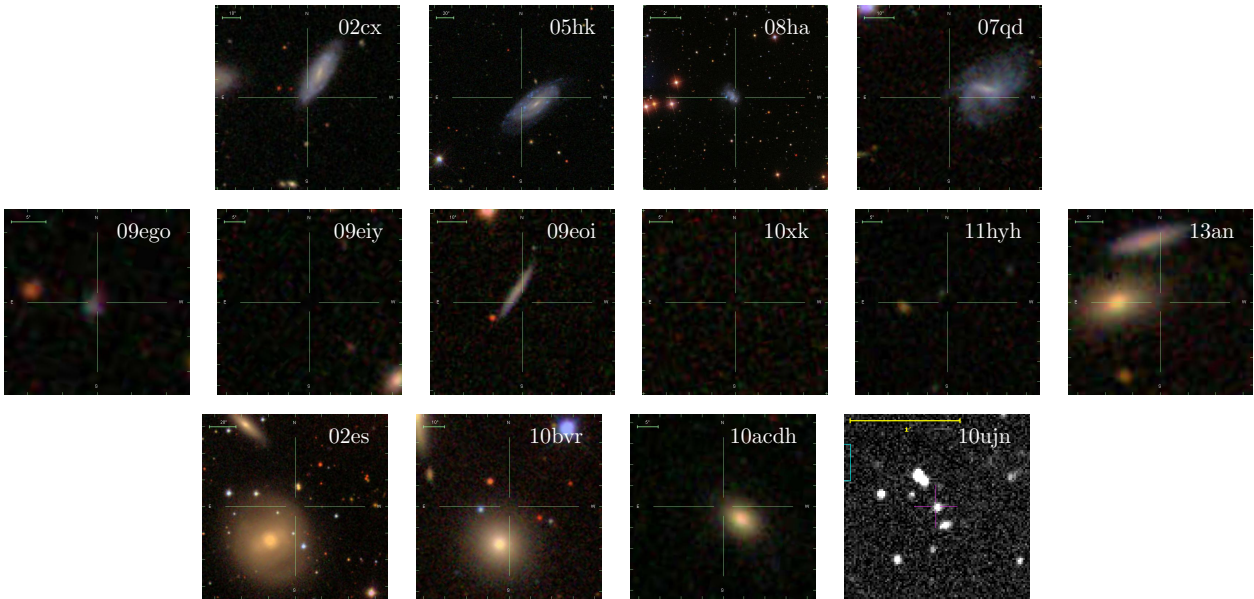


Fig. 6.— Images of hosts for 02cx-like and 02es-like objects. The top row shows four objects previously published in the literature. The second row shows the six 02cx-like objects in our sample. The bottom row shows the host for 02es itself (leftmost), followed by hosts for our three 02es-like objects. All images are from SDSS except for the host of PTF 10ujn, where the PTF reference image is used. All SDSS images are scaled so as to be 44 kpc on a side at the host’s distance, and the last image is 206 kpc on each side.

TABLE 3
HOST PROPERTIES

Name	Host	z^a	μ^b	$m(R)$ (mag) ^c	$M(R)$ (mag) ^d	$g-i$ (mag) ^e	Type ^f
Literature sample							
SN 1991bj	IC 344	0.018146	34.26	14.18	-20.08	...	Sb
SN 2002cx	CGCG 044-035	0.023963	35.18	15.39	-19.79	0.83	Sb
SN 2003gq	NGC 7407	0.021448	34.72	Sbc
SN 2004gw	PGC 16812	0.017018	34.28	Sbc
SN 2005hk	UGC 272	0.012993	33.53	14.42	-19.11	0.70	Sd
SN 2006hn	UGC 6154	0.017199	34.34	Sa
SN 2007qd	SDSS J020932.72-005959.7	0.043146	36.35	16.27	-20.08	0.59	Sc
SN 2008ge	NGC 1527	0.004043	31.12	10.25	-21.02	...	S0
SN 2008ha	UGC 12682	0.004647	30.83	14.03	-17.47	0.59	Irr
SN 2009ku	APMUKS(BJ) B032747.73-281526.1	0.0792	37.76	Sc
SN 2002es	UGC 2708	0.0182	34.42	13.22	-22.20	1.58	S0
SN 2002cx matches							
PTF 09ego	SDSS J172625.23+625821.4	0.104	38.40	20.45	-17.95	0.86	...
PTF 09eiy	...	(0.06)	37.14	>22.7	>-14.4
PTF 09eoi	SDSS J232412.96+124646.6	0.0415	36.30	17.60	-18.70	0.92	...
PTF 10xk	...	(0.066)	37.35	\gtrsim 23.5	\gtrsim -13.9
PTF 11hyh	SDSS J014550.57+143501.9	(0.057)	37.02	21.81	-15.21	0.90	...
iPTF 13an	2MASX J12141590+1532096	0.080315	37.70	16.58	-21.12	1.11	...
SN 2002es matches							
PTF 10bvr	CGCG 224-067 ^g	0.015	34.05	14.11	-19.94	1.26	E
PTF 10ujn	...	0.113	38.59	\approx 20	\approx -19
PTF 10acdh	2MASX J09430730+0939285	0.059471	37.06	16.63	-20.43	1.34	...
Other objects from literature							
SN 1991T	NGC 4527	0.005791	32.35	11.50	-19.16	2.07	Sb
SN 1991bg	M84	0.003392	31.17	9.88	-21.29	1.29	E
SN 2009dc	UGC 10064	0.021391	34.83	13.63	-21.20	1.33	S0

^aHeliocentric redshifts from the following sources: Catinella et al. 2005 (SN 1991bj), Falco et al. 111 (SNe 2002cx and 2009dc), de Vaucouleurs et al. 1991 (SN 2003gq), Paturel et al. 2003 (SN 2004gw), Barnes et al. 2001 (SN 2005hk), Fisher et al. 1995 (SN 2006hn), SDSS (SN 2007qd, iPTF 13an, PTF 10acdh), Ogando et al. 2008 (SN 2008ge), Lu et al. 1993 (SN 2008ha), Narayan et al. 2011 (SN 2009ku), Ganeshalingam et al. 2012 (SN 2002es), Strauss et al. 1992 (SN 1991T), Cappellari et al. 2011 (SN 1991bg). Otherwise the values are from PTF spectra (multiple narrow lines for PTF 09ego and 09eoi, Na D for PTF 10bvr, Na D and Ca IR for PTF 10ujn) or fits to SN 2002cx spectra (PTF 09eiy, 10xk, 11hyh).

^bDistance moduli taken to be as follows: the median redshift-independent value listed on NED, excluding any determinations made using the supernova in question (SNe 1991bj, 2003gq, 2008ge, 2008ha, 1991T, 1991bg); calculated from the CMB-frame redshift as reported on NED (all other literature objects except SN 2009ku); calculated from the heliocentric redshift (all remaining objects). Where necessary we assume $H_0 = 70.4 \text{ km s}^{-1} \text{ Mpc}^{-1}$, $\Omega_m = 0.273$, and $\Omega_\Lambda = 0.728$.

^cFrom Jones et al. 2009 (SN 1991bj), Lauberts & Valentijn 1989 (SN 2008ge), the PTF reference image (PTF 09eiy, 10xk, 10ujn), or SDSS (all others).

^dDefined as $m(R) - \mu$.

^eFrom SDSS.

^fWhere listed, morphological types are given in the following sources: Ganeshalingam et al. 2012 (SN 2002es), Narayan et al. 2011 (SN 2009ku), NED (PTF 10bvr), Lira et al. 1998 (SN 1991T), Filippenko et al. 1992 (SN 1991bg), Silverman et al. 2011 (SN 2009dc), Foley et al. 2009 (all others).

^gThis large elliptical galaxy is closest based on SDSS imaging and has a redshift of 0.03. However, here we employ a redshift of 0.015 based on narrow Na D found in the PTF spectrum of the transient.

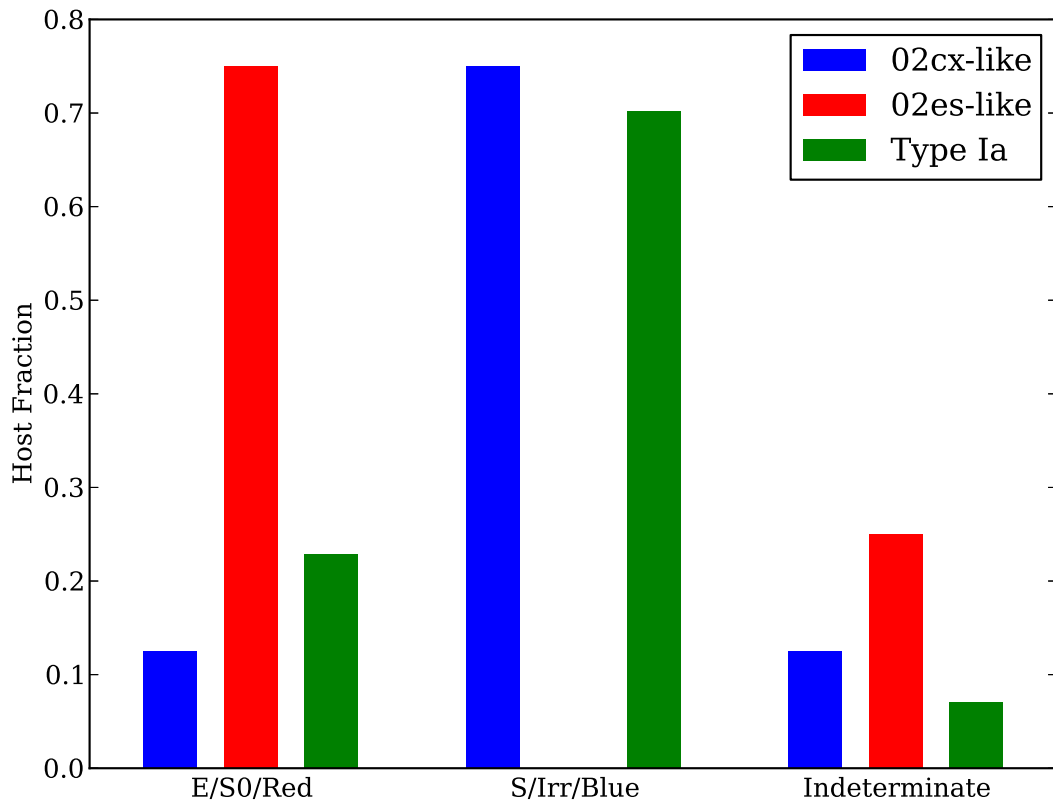


Fig. 7.— Distribution of host morphological types, with color used as a stand-in where the type is not published. The three distributions are calculated from sixteen (SN 2002cx), four (SN 2002es), and 57 (Type Ia) objects, the latter of which are given in Gallagher et al. (2005). Note that we are limited by small-number statistics with our sample.

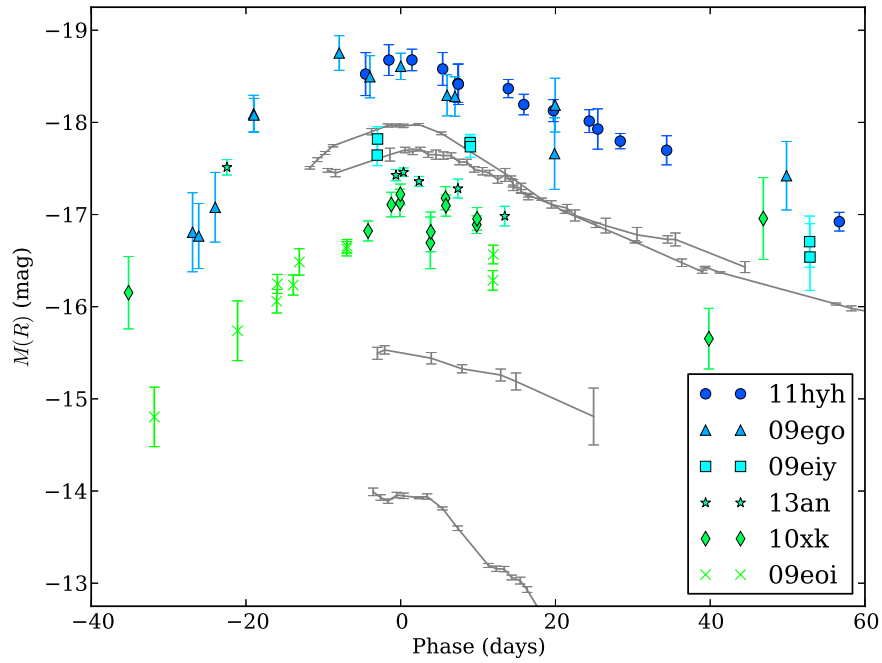


Fig. 8.— Light curves for the PTF sample. The gray curves show SNe 2005hk, 2002cx, 2007qd, and 2008ha from top to bottom, i.e. in order of decreasing peak luminosity.

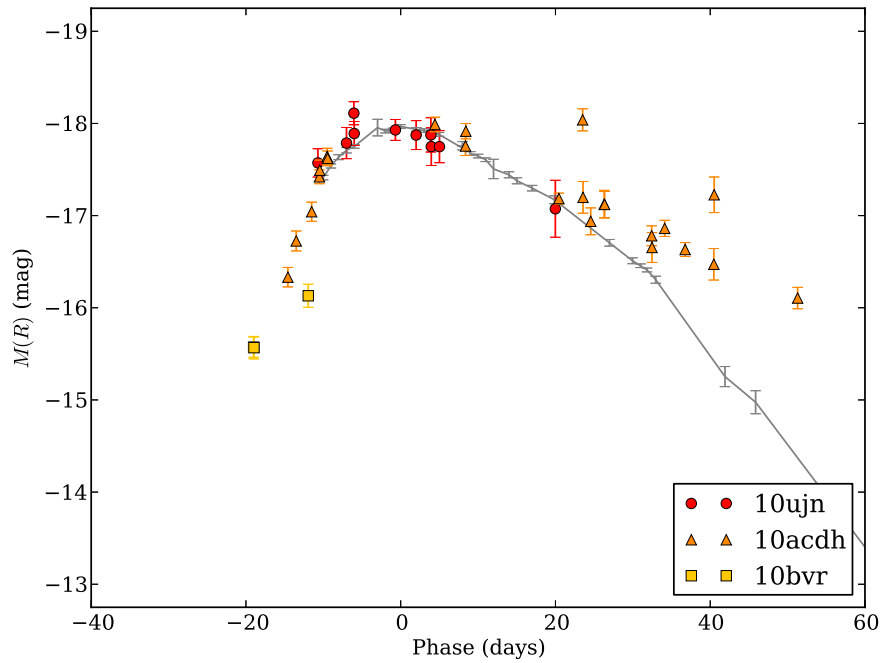


Fig. 9.— Light curves for the 02es-like objects in the PTF sample. The gray points are for SN 2002es itself. Note how close the peak magnitudes are to one another. In the case of PTF 10bvr, there is insufficient photometry to constrain the peak.

TABLE 4
LIGHT CURVE PROPERTIES IN R -BAND

Name	Peak MJD ^a	$M_{\text{peak}}(R)$ (mag) ^b	Rise Time (days)	$\Delta m_{15}(R)$ (mag)
Literature sample ^c				
SN 1991bj	≈ 48593.0
SN 2002cx	52421.2	-17.7	...	0.52
SN 2003gq	52854.5	-17.2	...	0.71
SN 2004gw	≈ 53362.0
SN 2005hk	53691.8	-18.0	20	0.67
SN 2006hn	≈ 54003.0
SN 2007qd	54408.4	-15.6	...	0.28
SN 2008ge	$\approx 54725.0^e$
SN 2008ha	54787.3	-14.2	...	0.97
SN 2009ku	55097.2	-18.5	...	0.32
SN 2002es	52521.0	-18.0	16	0.57
SN 2002cx matches				
PTF 09ego	55088.3	-18.3	26	0.25
PTF 09eiy	55084.4	< -18.0	...	0.38
PTF 09eoi	55076.3	-16.9	24	...
PTF 10xk	55203.3	-17.3	...	0.57
PTF 11hyh	55755.0	-18.7	...	0.44
iPTF 13an	$\approx 56328.0^f$	< -17.5 ^f	...	0.61 ^f
SN 2002es matches				
PTF 10bvr	55263.5	< -16.1
PTF 10ujn	55452.5	-17.9	17	0.63
PTF 10acdh	55553.0	-18.1	14	0.70
Other objects from literature ^d				
SN 1991T	48377.1	-19.2	16	0.60
SN 1991bg	48605.5	-17.5	...	1.36
SN 2009dc	54946.9 ^g	-19.5	23	0.15

^aModified Julian Date, $\text{MJD} = \text{JD} - 2,400,000$.

^bUses distance moduli as reported in Table 3.

^cDerived from data from the following sources: Foley et al. 2013 (SNe 1991bj, 2003gq, 2004gw, 2006hn, 2008ge), Li et al. 2003 (SN 2002cx), Sahu et al. 2008 (SN 2005hk), McClelland et al. 2010 (SN 2007qd), Foley et al. 2009 (SN 2008ha), Narayan et al. 2011 (SN 2009ku), Ganeshalingam et al. 2012 (SN 2002es).

^dDerived from data from the following sources: Lira et al. 1998 (SN 1991T), Filippenko et al. 1992 (SN 1991bg), Silverman et al. 2011 (SN 2009dc).

^ePeak in V -band.

^fAssuming earliest observation corresponds to peak brightness.

^gPeak in B -band.

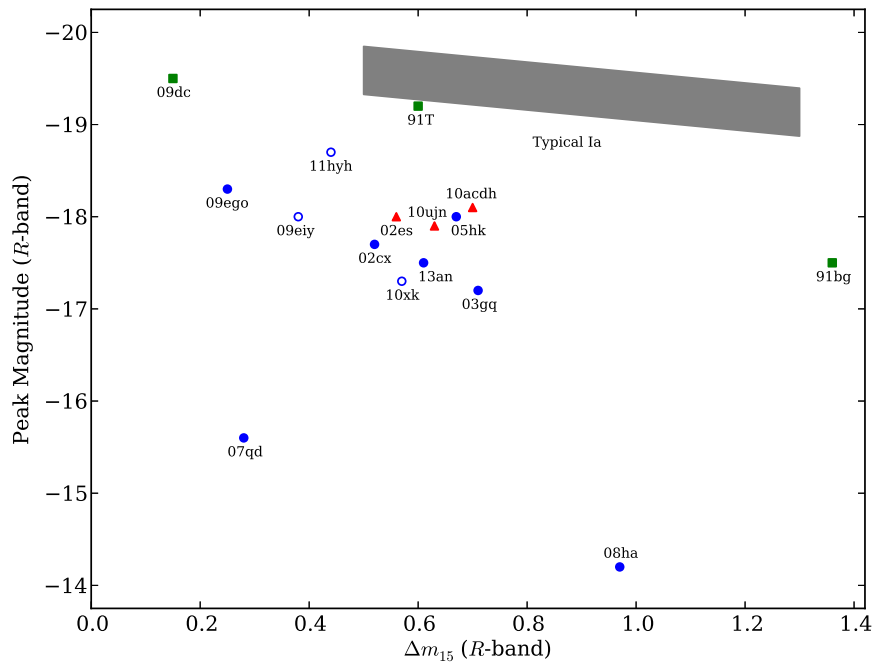


Fig. 10.— Relation between peak luminosity and decline rate in R -band (see Table 4). Blue circles indicate 02cx-like data, red triangles are for 02es-like objects, and green squares denote other supernovae discussed in the text. Open symbols denote some doubt regarding the host redshift. The gray band shows the Phillips relation in R -band with parameters obtained from Table 3 of Prieto et al. (2006), extrapolated to $\Delta m_{15} = 0.5$ and truncated at $\Delta m_{15} = 1.3$. In particular, this region shades a 2σ scatter about the best-fit line.

TABLE 5
OBSERVATIONS OF SPECTRA

Name	Date (UT)	MJD	Phase ^a (days)	Telescope	Instrument	Wavelength Range (Å)
PTF 09ego	2009-09-23	55097.9	+9	Keck 1	LRIS	3800–9200
	2010-05-15	55332	+221	Keck 1	LRIS	3400–8800
PTF 09eiy	2009-09-23	55097.9	+14	Keck 1	LRIS	3500–9700
	2009-10-12	55117	+33	WHT	ISIS	3800–7600
	2009-11-11	55147.0	+63	Keck 1	LRIS	3700–8700
	2009-12-19	55184.8	+100	Keck 1	LRIS	3800–8800
	2010-01-09	55205.8	+121	Keck 1	LRIS	3900–8000
PTF 09eoi	2009-09-23	55098.0	+21	Keck 1	LRIS	3700–9600
	2009-10-11	55116	+38	WHT	ISIS	3800–7800
	2009-10-16	55120.7	+43	Keck 1	LRIS	3500–8400
	2009-11-11	55146.8	+68	Keck 1	LRIS	3700–8900
	2009-12-19	55184.7	+104	Keck 1	LRIS	4000–8000
PTF 10xk	2010-02-11	55238.8	+36	Keck 1	LRIS	3500–9100
	2010-03-07	55262.8	+60	Keck 1	LRIS	3500–7200
PTF 10bvr	2010-03-07	55263.1	+9	Keck 1	LRIS	3500–9000
PTF 10ujn	2010-11-07	55508.1	+56	Keck 1	LRIS	3900–8300
PTF 10acdh	2010-12-13	55544	–8	P200	DBSP	3800–8000
	2010-12-30	55561	+8	Keck 1	LRIS	3500–9500
PTF 11hyh	2011-08-06	55780.0	+25	P200	DBSP	3600–8800
iPTF 13an ^b	2013-02-18	56341.9	+13	P200	DBSP	3100–9300
	2013-06-06	56450	+113	Keck 2	DEIMOS	4500–8900

^aTime since *R*-band maximum; adjusted for host redshift except in the cases of PTF 09eiy, 10xk, and 11hyh.

^bPhases given are lower bounds, as observations began after maximum.

TABLE 6
RELATIVE VELOCITIES COMPARED TO TEMPLATES

Object	Phase (days) ^a	Velocity (km s ⁻¹) Relative to					
		SN 2002cx +12 (7000 km s ⁻¹)	SN 2002cx +25 (5000 km s ⁻¹)	SN 2002cx +56 (2000 km s ⁻¹)	SN 2005hk +54	SN 2008ha +11	SN 2002es +6 (6000 km s ⁻¹)
Templates							
SN 2002cx	+12	-4	+1070	+1811	+2270	+3041	-140
	+25	-1096	-6	+857	+948	+1925	-1901
	+56	-1813	-844	-5	+140	+873	-2239
SN 2005hk	+4	+895	+2405	+3100	+3003	+4844	+503
	+54	-2278	-963	-142	-4	+771	-2888
SN 2008ha	+8	-3118	-1752	-870	-655	+151	-3467
	+11	-2908	-1843	-878	-761	-2	-3304
	+22	-3979	-2920	-1645	-1561	-243	-3974
SN 2002es	+6	+183	+1904	+2252	+2873	+2362	-3
	+67	-539	-200	+683	+862	+2040	-97
02cx-likes							
SN 1991bj	≈ +29	-1050	+158	+1044	+1277	+3635	-577
	≈ +39	+4025	+5120	+6236	+6365	+7907	+2464
SN 2003gq	-6	+2972	+3928	+3594	+5260	+4376	+1034
	-4	+1881	+4336	+4752	+5553	+3854	+195
	+55	-2386	-1549	-1083	-683	...	-2797
SN 2004gw	≈ +24	-85	+948	+2024	+2103	+3783	-694
	≈ +52	-1279	-221	+764	+926	+2416	-1148
SN 2006hn	≈ +30	-1284	-144	+750	+1115	...	-2095
SN 2007qd	+10	-2303	-986	+42	+211	+625	-2806
	+14	-3124	-1650	-675	-410	+134	-3370
SN 2008ge	+41	-677	+500	+1628	+1740	+2600	-1756
PTF 09ego	+9	-283	+254	+181	+175	+1438	-1025
	+221	-879	-751	-266	-445	-60	+53
PTF 09eiy ^b	+14	+2642	+3637	+4403	+4885	+4740	+1380
	+33	-295	+222	+961	+1020	+1944	-1594
	+63	-1709	-1276	-388	-260	+360	-2712
	+100	-2970	-2200	-1174	-964	-500	-3895
	+121	-3110	-2581	-1501	-1403	-495	-3671
PTF 09eoi	+21	-1583	-530	+479	+624	+1100	-2375
	+38	-2176	-1468	-486	-503	+456	-3043
	+43	-2522	-1254	-266	-166	+477	-2824
	+68	-2782	-1222	-392	-234	+156	-3163
+104	-2284	+518	-273	-117	+276	+637	
PTF 10xk ^b	+36	-1902	-804	+151	+311	+1302	-2312
	+60	-1955	-1031	-191	+188	+790	-1185
PTF 11hyh ^b	+25	-1113	-62	+554	+719	+1544	-1590
iPTF 13an	+13 ^c	-683	+567	+1590	+1685	+2139	-1539
	+113 ^c	-2541	-1500	-701	-483	+170	-2625
02es-likes							
PTF 10bvr	+9	-1457	-239	-252	-664	+2594	-1952
PTF 10ujn	+50	-508	+400	+966	+1302	+2003	-822
PTF 10acdh	-8	+7782	+8777	+9894	+10353	+10503	+2334
	+8	+2086	+2764	+3098	+3270	+4284	+865
Other objects from literature							

TABLE 6—*Continued*

Object	Phase (days) ^a	Velocity (km s ⁻¹) Relative to					
		SN 2002cx +12 (7000 km s ⁻¹)	SN 2002cx +25 (5000 km s ⁻¹)	SN 2002cx +56 (2000 km s ⁻¹)	SN 2005hk +54	SN 2008ha +11	SN 2002es +6 (6000 km s ⁻¹)
SN 1991T	+6	+5500	+6730	+7797	+7988	+7809	+4330
	+40	+3648	+4536	+5534	+5763	+7390	+2569
SN 1991bg	0	+10947	+12124	+12936	+12978	+14192	+2990
	+53	+2134	+3360	+3463	+3975	+5570	+2441
SN 2009dc	-7	+4837	-2202	-1203	-1439	+402	+2389
	+23	+611	+1390	+1152	+2594	+3958	+505
	+35	-818	+199	+961	+1412	...	-827
	+52	-1114	-211	-61	+644	...	-923
	+64	-646	-15	+147	+832	+3083	-250
	+79	-123	+420	+762	+1378	+3009	-217
	+80	-368	+241	+640	+1256	+2829	-158
	+87	-23	+479	+923	+1597	+2897	-358
	+92	+8	+580	+930	+1622	+2877	-149
	+109	+147	+635	+1090	+1829	+2330	-1636
	+281	-2318	-1317	0	+549	+1302	-2024
	SN 2011fe	+7	+4869	+6858	+9519	+8943	+5290
+16		+2915	+3660	+4140	+5018	+5316	+2520
+78		+3227	+1932	+2303	+2782	+4198	+956

^aTime since *R*-band maximum; adjusted for host redshift except in the cases of PTF 09ey, 10xk, and 11yh.

^bShift depends on chosen value for redshift.

^cAssuming first observation corresponds to peak luminosity.

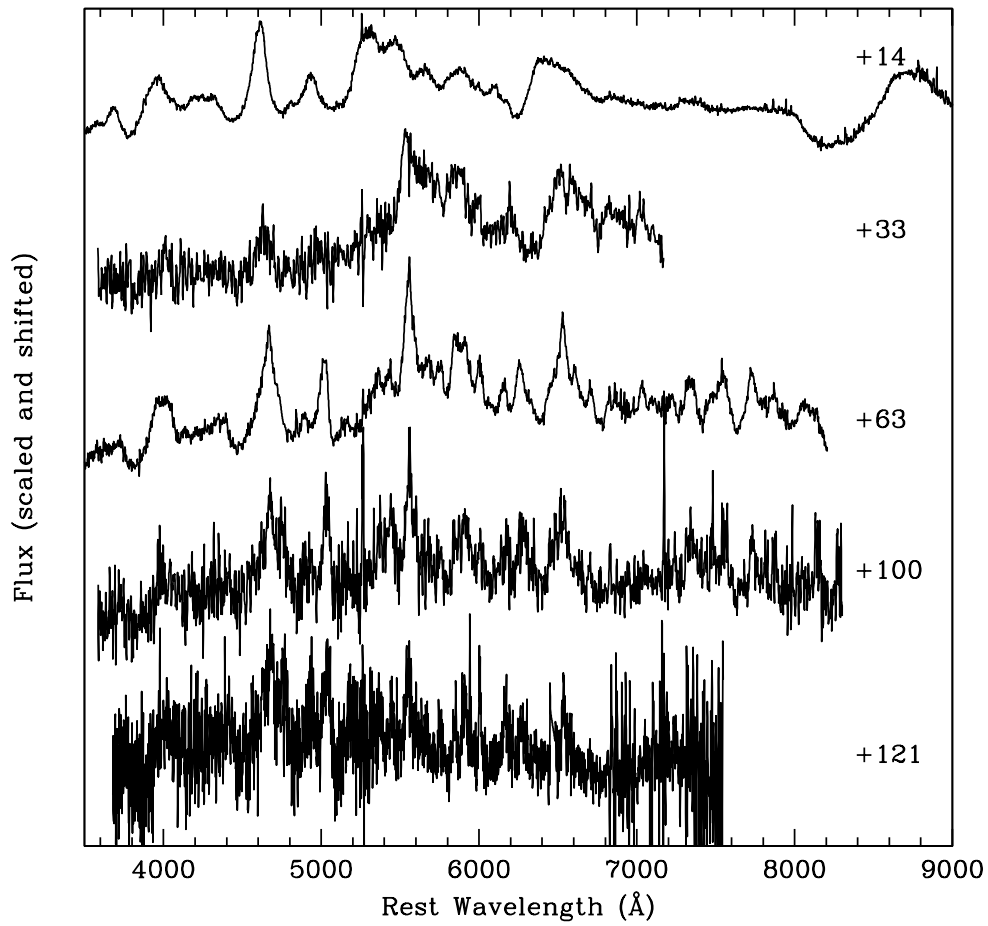


Fig. 11.— Spectral evolution of PTF 09ey. Phases labeled are days after peak *R*-band brightness, as defined in Table 4. Details of observations can be found in Table 5.

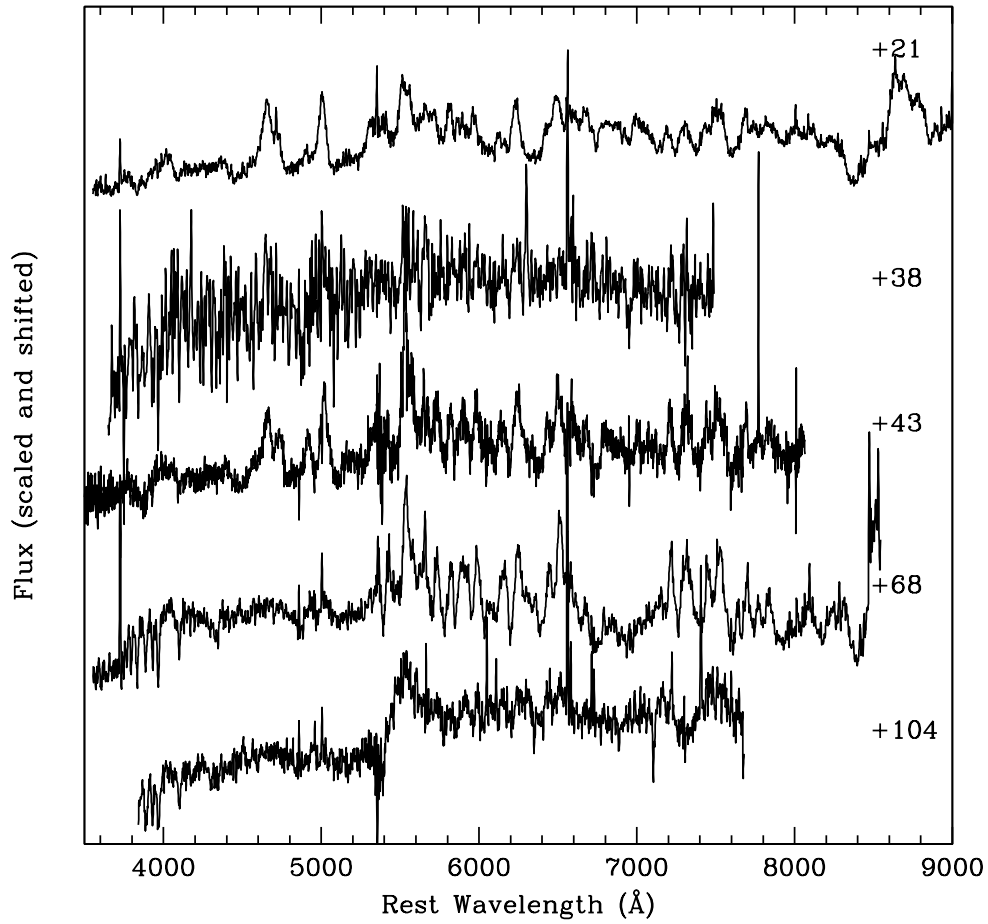


Fig. 12.— Spectral evolution of PTF 09eoi. Phases labeled are days after peak R -band brightness, as defined in Table 4. Details of observations can be found in Table 5.

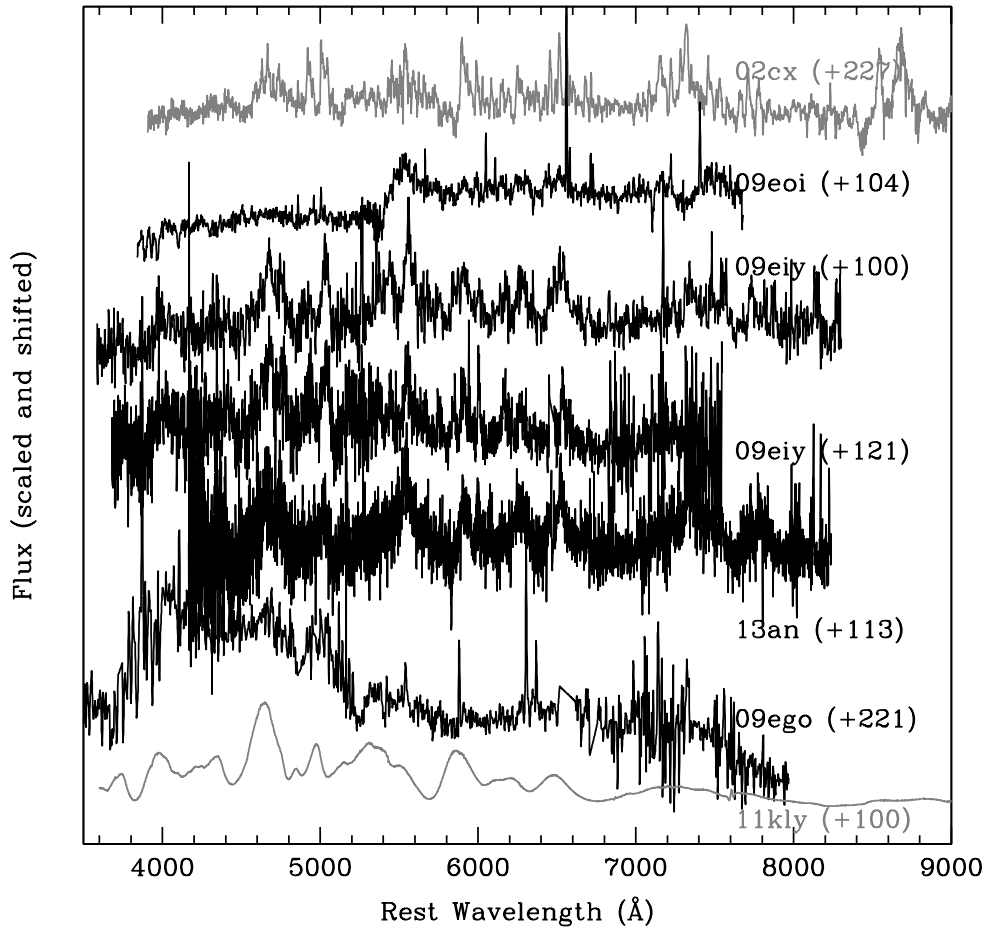


Fig. 13.— Montage of late-time spectra. SN 2002cx (Jha et al. 2006) is shown on top, with a typical SN Ia shown at the bottom. Details of observations can be found in Table 5.

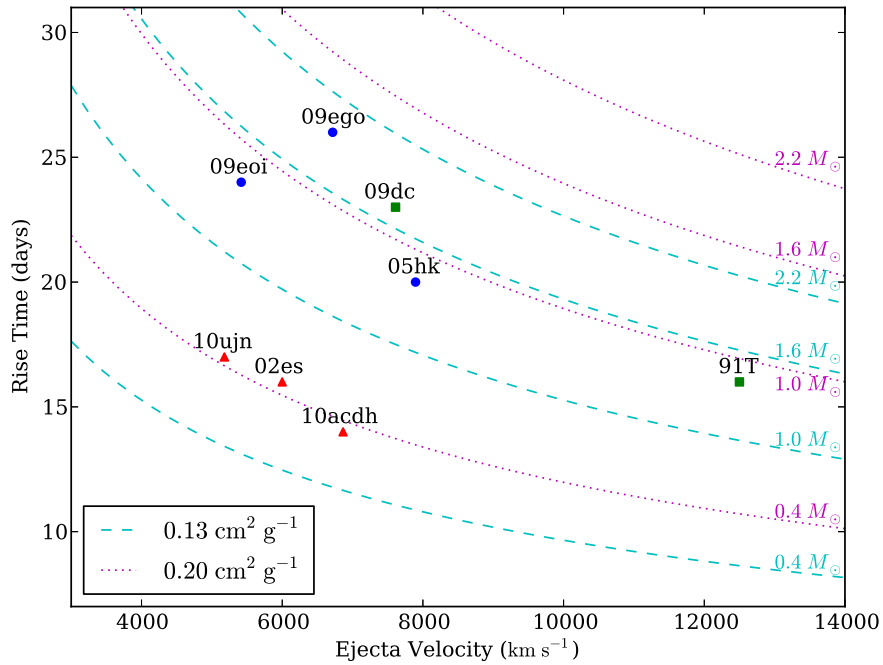


Fig. 14.— Visualization of Arnett’s Law. The symbol scheme is the same as in Figure 10. Lines of constant ejecta mass are calculated for two different values of effective opacity. The rise time for SN 2009dc is taken from Silverman et al. (2011); all others are calculated as described in the text.

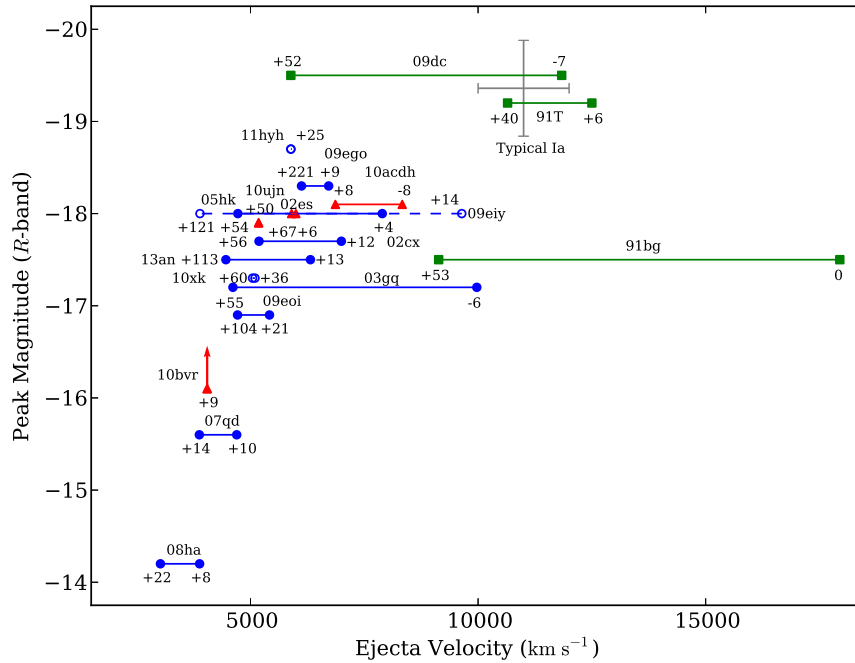


Fig. 15.— Relation between peak luminosity in R band (see Table 4) and ejecta velocity (see Table 6). The symbol scheme is the same as in Figure 10. Typical SNe Ia have velocities of 10,000–12,000 km s^{-1} . The typical peak magnitudes are obtained by projecting the relation in Figure 10.

TABLE 7
 PROPERTIES OF SN 2002CX AND SN 2002ES FAMILIES

Property	02cx-like	02es-like
Host type	generally late	early
Host $g-i$ color (mag)	0.59–1.47	1.26–1.58
Host luminosity (R -band, mag)	–14 to –21	–19 to –22
Peak luminosity (R -band, mag)	–13 to –19	–18
Rise time (days)	20–30	14–17
Decline rate (Δm_{15} , mag)	0.2–1.0	0.6–0.7
Ti II trough?	no	yes
Ejecta velocity (km s^{-1}) ^a	4000–9000	4000–7000

^aAt approximately 10 days post-maximum.

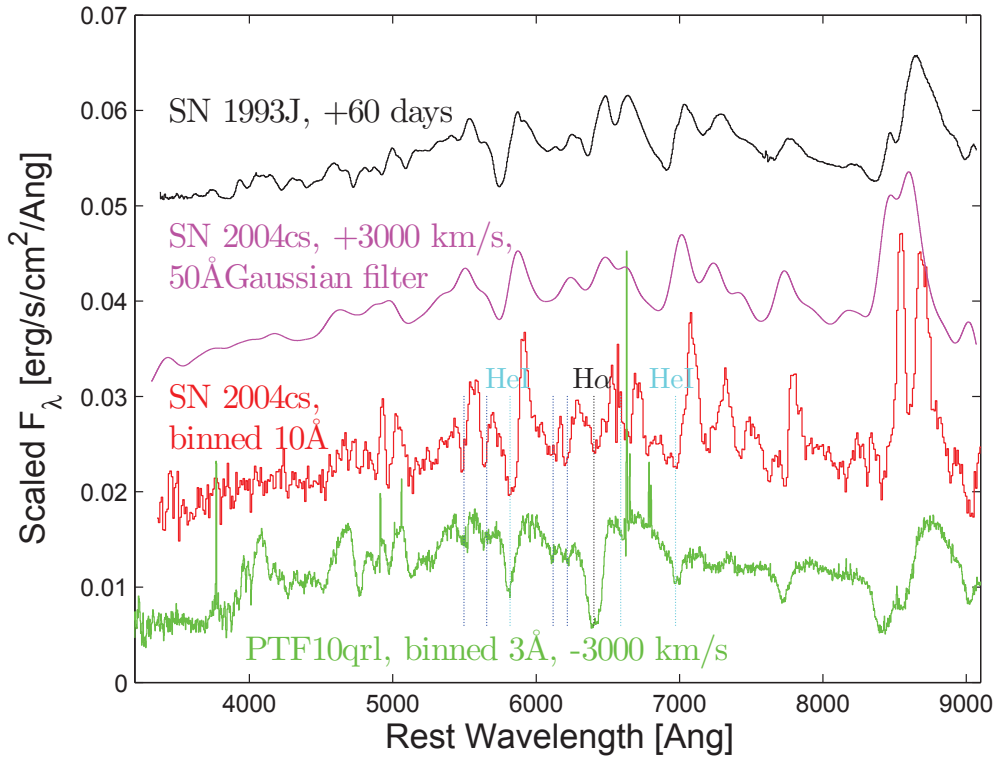


Fig. 16.— Comparison of spectra of SN 2004cs (red) and PTF 10qrl (green, a low-velocity SN IIB) showing excellent alignment of features. Absorption lines of hydrogen ($H\alpha$, black) and He I (5876 Å and 7065 Å, cyan) are clearly identified, and additional nearby features (blue) also perfectly align. A broadened and blueshifted version of the SN 2004cs spectrum (magenta) also displays a strong similarity to a spectrum of the prototypical Type IIB SN 1993J (black).

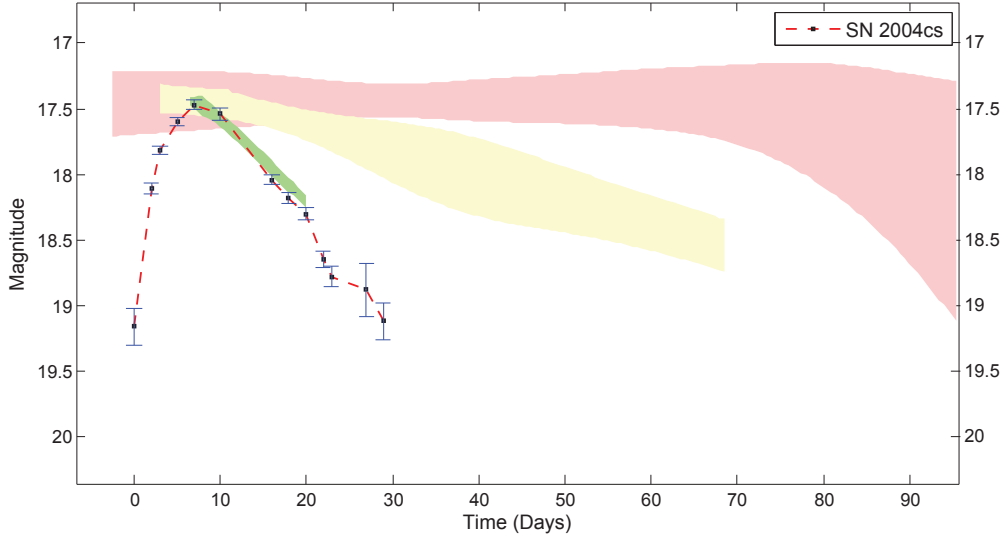


Fig. 17.— Unfiltered photometry of SN 2004cs (Foley et al. 2013) fitting the R -band SN IIB template (green shade) from Arcavi et al. (2012). The yellow band indicates Type IIL SNe II, while the pink represents Type IIP.

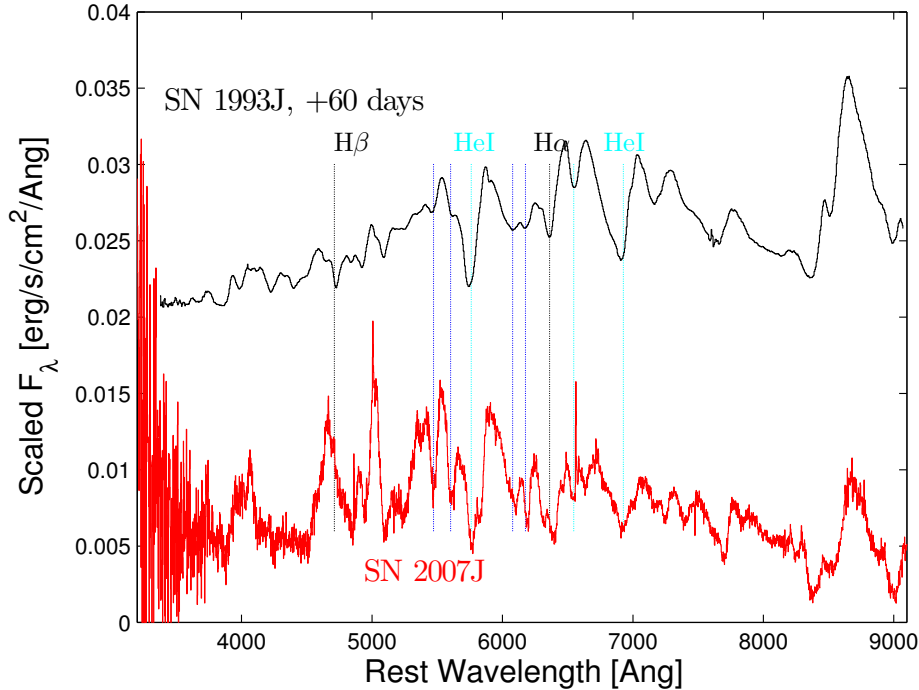


Fig. 18.— Comparison of the spectrum of SN 2007J (red) with that of SN 1993J (black). The $H\alpha$ (black) and He I (5876 Å and 7065 Å, cyan) lines are clearly identified, and additional nearby features (blue) align as well. $H\beta$ is not detected in SN 2007J, perhaps indicating a thinner hydrogen envelope.

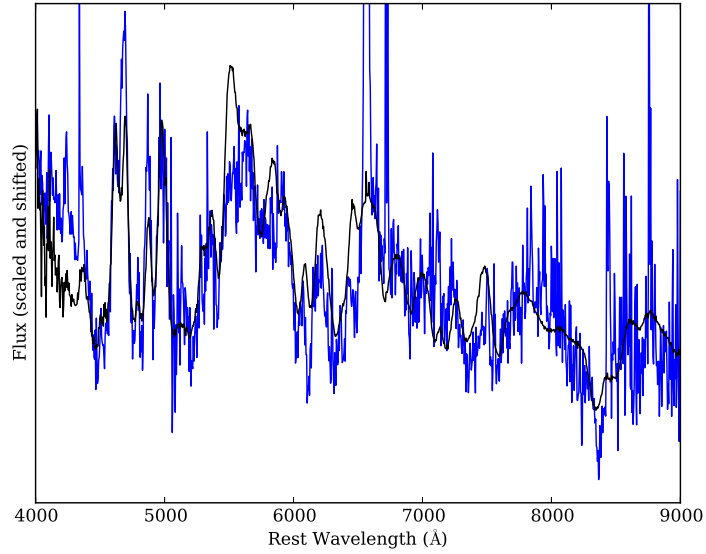


Fig. 19.— Comparison between PTF 09ego (blue, +9 days) and SN 2002cx (black, +20 days). The former has had galaxy light subtracted via Superfit.

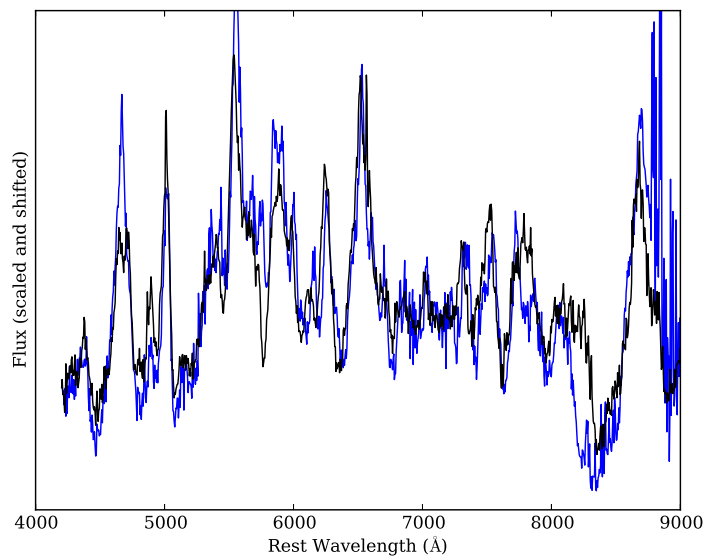


Fig. 20.— Comparison between PTF 09eyi (blue, +55 days) and SN 2002cx (black, +56 days). The former has had galaxy light subtracted via Superfit, and the fiducial redshift of 0.06 was used to align spectra.

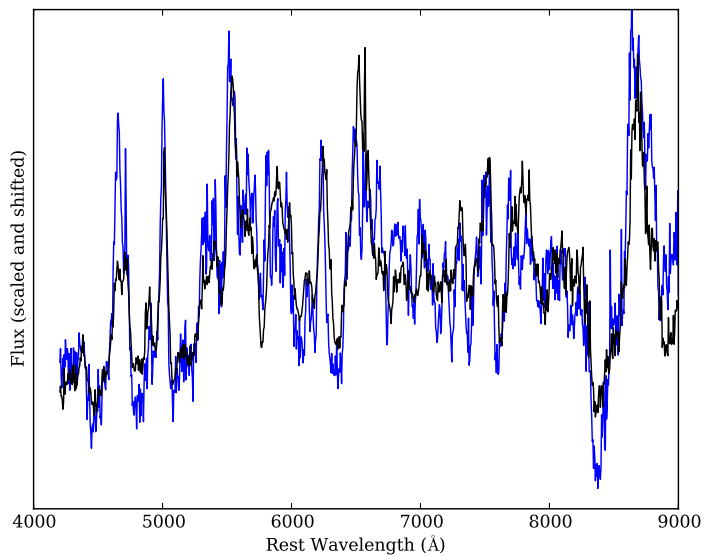


Fig. 21.— Comparison between PTF 09eoi (blue, +21 days) and SN 2002cx (black, +56 days). The former has had galaxy light subtracted via Superfit.

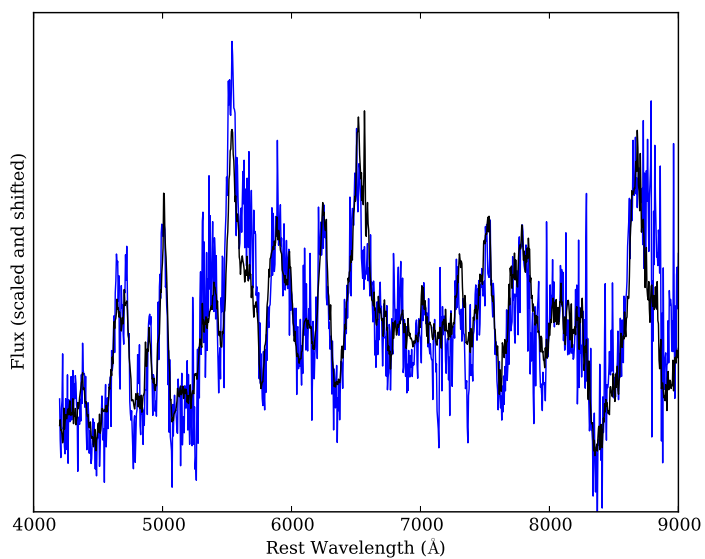


Fig. 22.— Comparison between PTF 10xk (blue, +36 days) and SN 2002cx (black, +56 days). The former has had galaxy light subtracted via Superfit, and the fiducial redshift of 0.066 was used to align spectra.

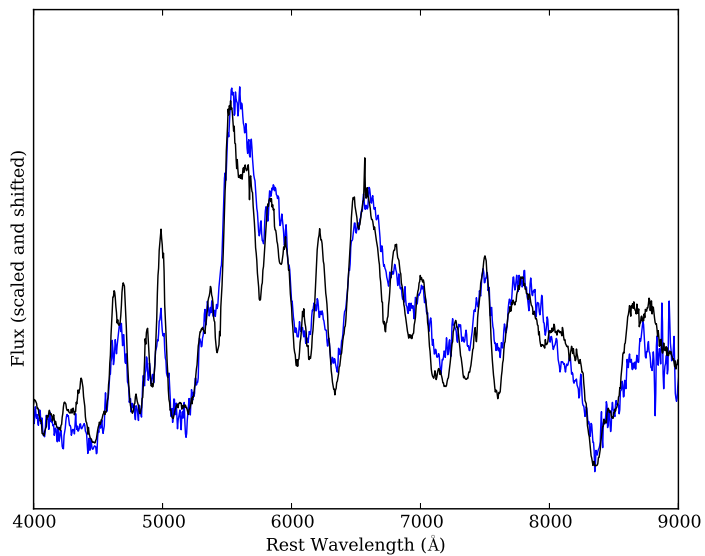


Fig. 23.— Comparison between PTF 11hyh (blue, +25 days) and SN 2002cx (black, +25 days). The former has had galaxy light subtracted via Superfit, and the fiducial redshift of 0.057 was used to align spectra.

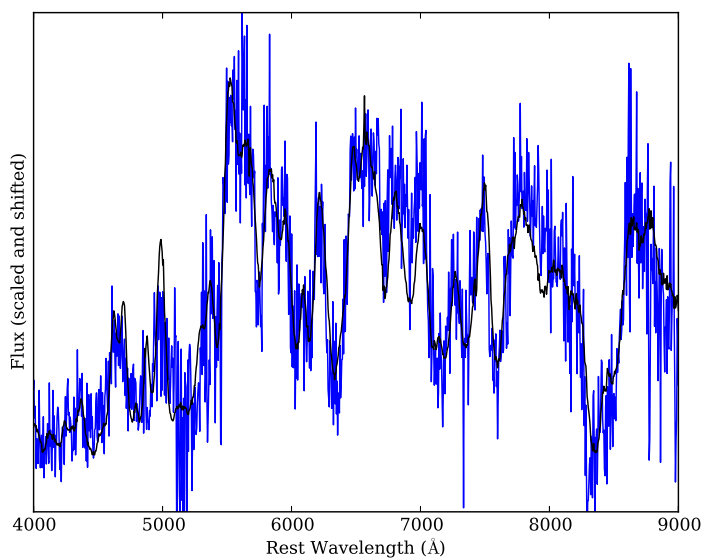


Fig. 24.— Comparison between iPTF 13an (blue, at least +13 days) and SN 2002cx (black, +25 days). The former has had galaxy light subtracted via Superfit.

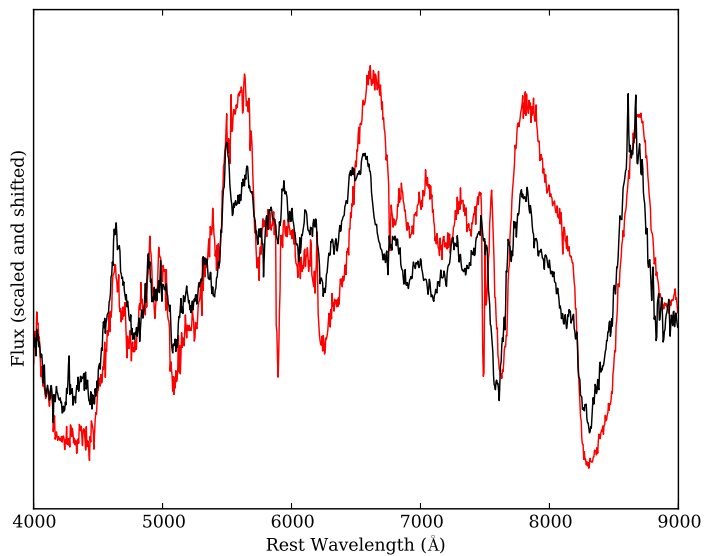


Fig. 25.— Comparison between PTF 10bvr (red, +9 days) and SN 2002es (black, +13 days). The former has had galaxy light subtracted via Superfit.

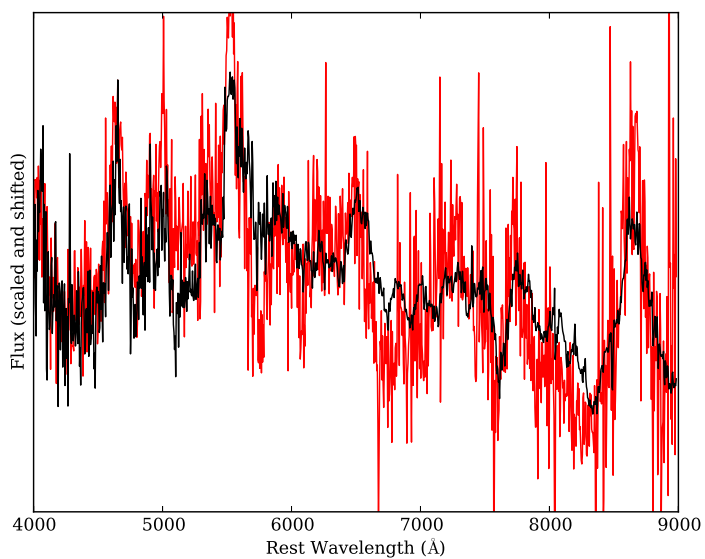


Fig. 26.— Comparison between PTF 10ujn (red, +56 days) and SN 2002es (black, +30 days). The former has had galaxy light subtracted via Superfit.

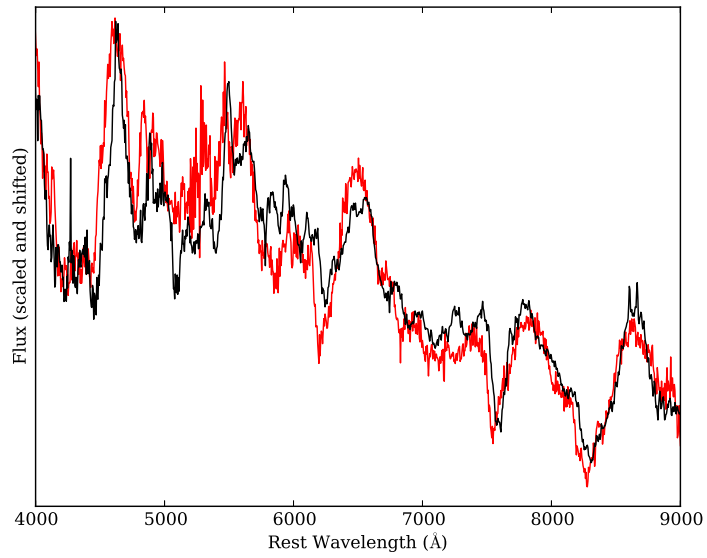


Fig. 27.— Comparison between PTF 10acdh (red, +8 days) and SN 2002es (black, +13 days). The former has had galaxy light subtracted via Superfit.

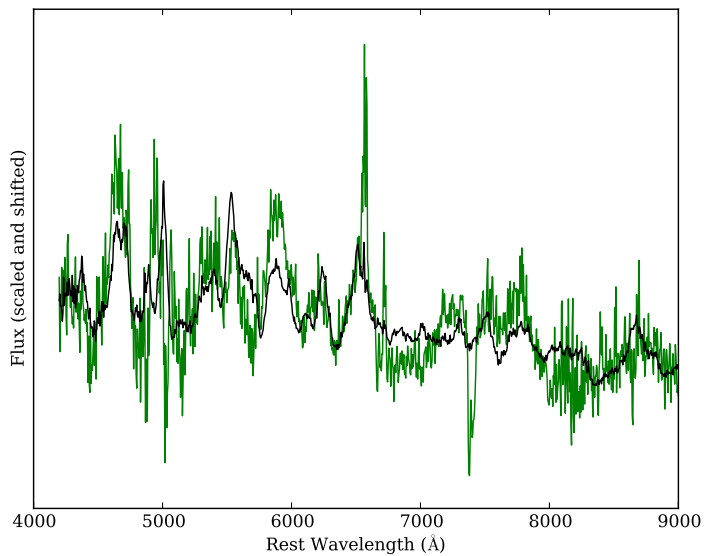


Fig. 28.— Comparison between PTF 10vzj (green, +51 days) and SN 2002cx (black, +56 days). The former has had galaxy light subtracted via Superfit.

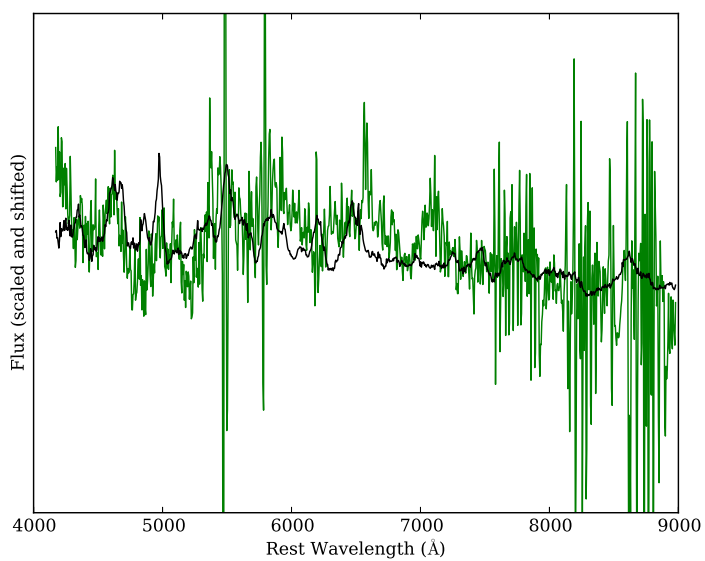


Fig. 29.— Comparison between PTF 10xfh (green, unknown phase, spectrum taken 2010 October 8) and SN 2002cx (black, +56 days). The former has had galaxy light subtracted via Superfit.

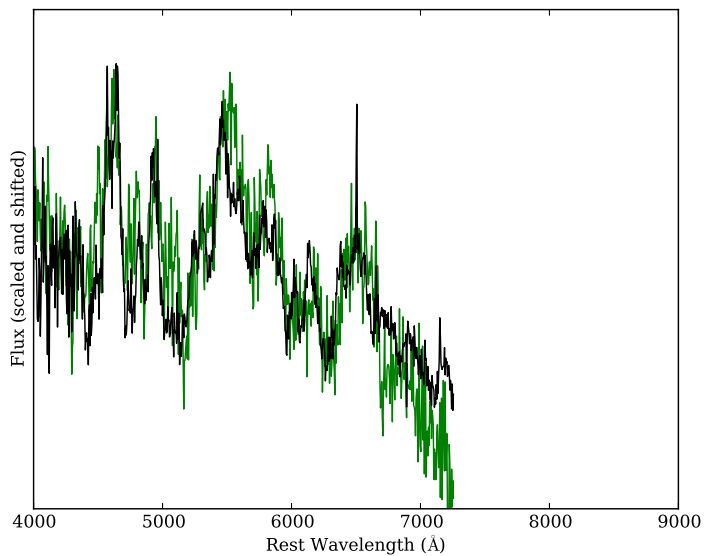


Fig. 30.— Comparison between PTF 11cfm (green, +24 days) and SN 2002cx (black, +15 days). The former has had galaxy light subtracted via Superfit.

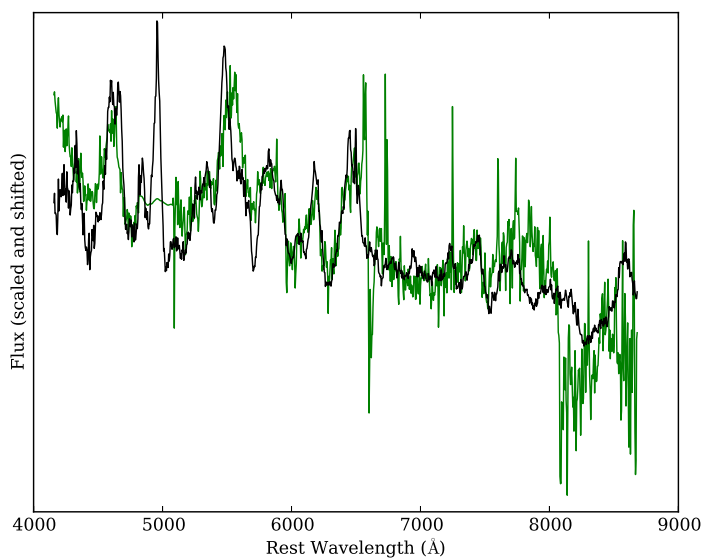


Fig. 31.— Comparison between PTF 11pzq (green, +18 days) and SN 2002cx (black, +56 days). The former has had galaxy light subtracted via Superfit.

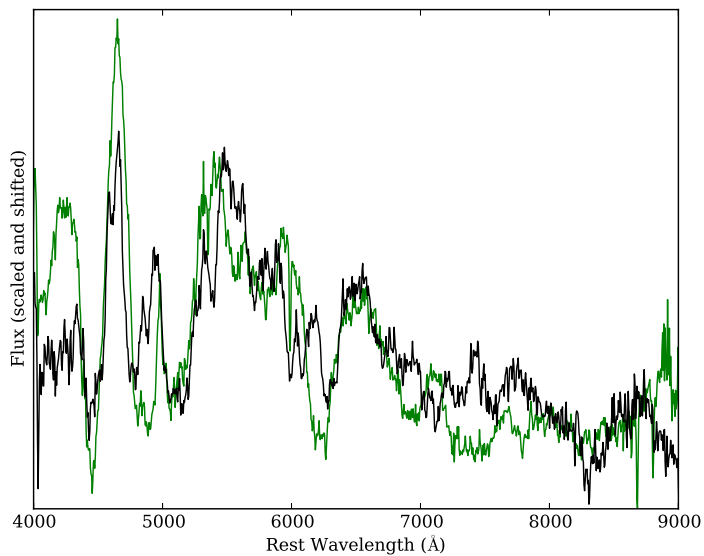


Fig. 32.— Comparison between PTF 09aly (green, +6 days) and SN 2005hk (black, +15 days). The former has had galaxy light subtracted via Superfit.

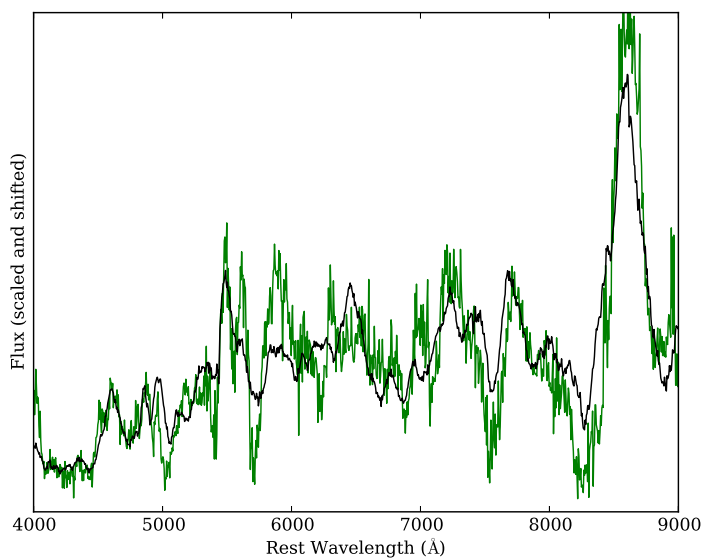


Fig. 33.— Comparison between PTF 09dav (green, +12 days) and SN 2002es (black, +37 days). The former has had galaxy light subtracted via Superfit.

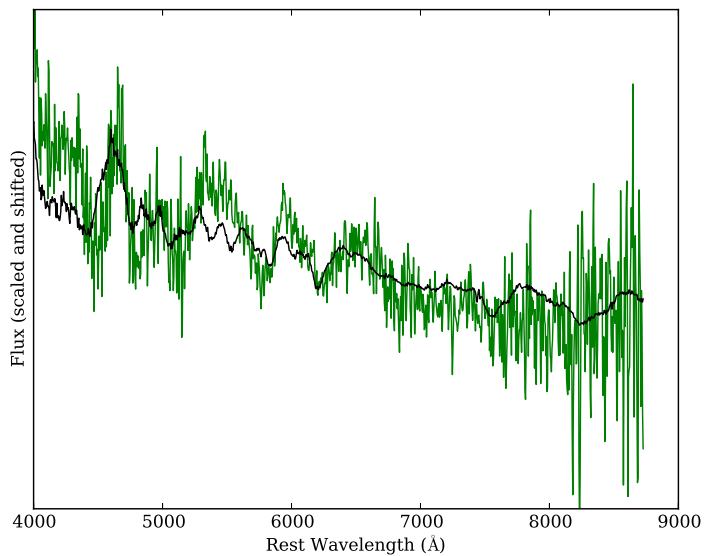


Fig. 34.— Comparison between PTF 10pko (green, +8 days) and SN 2002es (black, +3 days). The former has had galaxy light subtracted via Superfit.

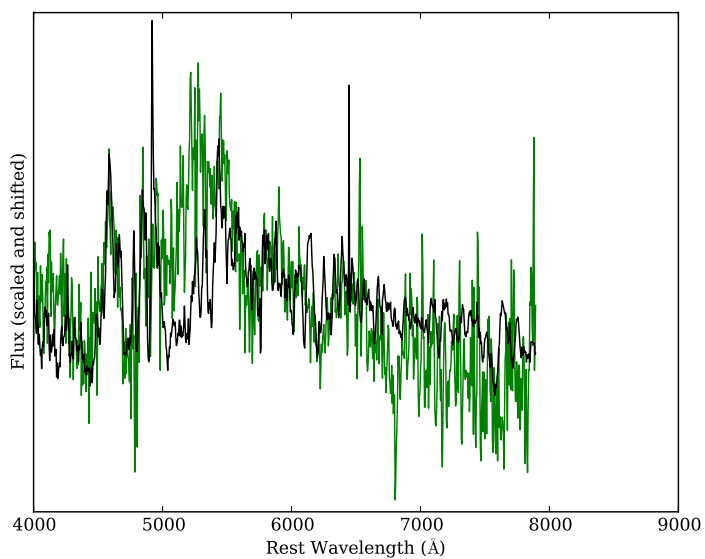


Fig. 35.— Comparison between PTF 10xfv (green, +17 days) and SN 2008ha (black, +11 days). The former has had galaxy light subtracted via Superfit.

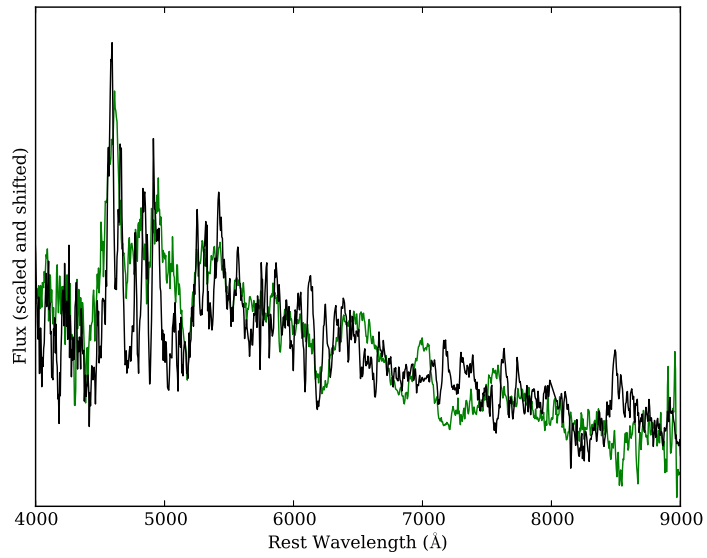


Fig. 36.— Comparison between PTF 11sd (green, +8 days) and SN 2008ha (black, +8 days). The former has had galaxy light subtracted via Superfit.